buildings

MDPI

Article

Utilising High-Ambient-Temperature Curing in the Development of Low-Calcium Geopolymers

Cemal Karaaslan [1,2,*], Şeyda Şek [3] and Canan Turan [4]

[1] Igdir Vocational School of Technical Sciences, Igdir University, 76000 Igdir, Turkey
[2] Department of Civil Engineering, Faculty of Engineering, Igdir University, 76000 Igdir, Turkey
[3] Civil Engineering Department, Postgraduate Education Institute, Igdir University, 76000 Igdir, Turkey; o221101000004@ogr.igdir.edu.tr
[4] Department of Civil Engineering, Faculty of Engineering and Architecture, Kirsehir Ahi Evran University, 40100 Kirsehir, Turkey; canan.turan@ahievran.edu.tr
* Correspondence: cemal.karaaslan@igdir.edu.tr or cemalkaraas@gmail.com; Tel.: +90-0476-223-00-10

Abstract

Geopolymers are typically cured either at ambient temperature (~25 °C) or subjected to short-term heat curing before being stored under ambient conditions until testing. However, in hot-arid regions, the daily ambient temperature may exceed 45 °C during summer months. Therefore, such conditions should also be considered as high ambient curing, and their influence on low-calcium geopolymer performance needs to be investigated. In this study, pumice- and fly ash-based geopolymer mortars were produced to evaluate the effects of different curing regimes. In the pumice-based mixtures, 10 wt% of pumice was replaced with metakaolin to enrich the alumina content. Three curing conditions were applied: ambient curing, high ambient curing, and heat curing. Setting times of geopolymers were determined based on each curing regime. Physical properties, including density, water absorption, and sorption coefficient, were assessed. Compressive strength development was evaluated over 90 days. In addition, durability performance was assessed through water resistance, freeze–thaw durability, and resistance against sulphuric and hydrochloric acid. Fourier transform infrared spectroscopy and X-ray diffraction confirmed that geopolymerisation reactions continued significantly up to 90 days under high ambient curing, while mercury intrusion porosimetry showed a reduction in porosity. These findings explain the continuous increase in compressive strength. Pumice-based geopolymers cured under this condition exhibited significantly better long-term strength than those cured under other regimes. High ambient-cured fly ash-based geopolymers, a 3-day strength of 40.3 MPa was achieved, eliminating the need for heat curing. Thus, high ambient curing enables the in situ use of these geopolymers and offers a cost-effective and eco-friendly alternative.

Keywords: high-ambient-temperature curing; fly ash; pumice; geopolymers; durability; water resistance

Academic Editor: Mijia Yang

Received: 27 July 2025
Revised: 18 August 2025
Accepted: 19 August 2025
Published: 21 August 2025

Citation: Karaaslan, C.; Şek, Ş.; Turan, C. Utilising High-Ambient-Temperature Curing in the Development of Low-Calcium Geopolymers. *Buildings* **2025**, *15*, 2974. https://doi.org/10.3390/buildings15162974

Correction Statement: This article has been republished with a minor change. The change does not affect the scientific content of the article and further details are available within the backmatter of the website version of this article.

1. Introduction

The production of Ordinary Portland Cement (OPC) continues to increase globally due to the rising population and the growing demand for new residential and infrastructure developments. However, OPC production generates a significant amount of CO_2 emissions, leading to severe environmental challenges [1,2]. By 2030, global OPC production is projected to reach 4.80 billion tons [3]. This substantial increase is regarded as a major contributing factor to the ongoing climate change crisis, one of the most pressing global

challenges of the modern era. Therefore, the use of more sustainable and environmentally friendly materials, which also contribute to the circular economy, is becoming increasingly widespread [4].

Geopolymer cement has emerged as a competitive alternative to conventional OPC in recent years. Its lower carbon emissions, contribution to sustainability through the recycling of waste materials, high-early strength, and superior resistance to acid and sulphate attacks make it a promising substitute [5–8]. Geopolymers are generally defined as amorphous aluminosilicate-based materials, with their formation determined by the geopolymerisation mechanism [9]. This mechanism requires two essential components: raw materials with a high aluminosilicate content and an alkaline solution [10]. The sufficient presence of aluminosilicate in the raw materials ensures their effectiveness as precursors, facilitating a more efficient geopolymerisation process [4]. Within the scope of sustainability, by-products derived from industrial and agricultural waste with high aluminosilicate content, as well as certain naturally occurring materials, can be preferred as precursors [11]. Among the most commonly used industrial by-products are fly ash and ground granulated blast furnace slag [3], while naturally sourced materials, depending on geographical availability, include pumice, kaolinite, and calcined clays [10]. The alkali solutions required for the geopolymerisation mechanism to occur are typically composed of sodium-based (sodium hydroxide and/or sodium silicate) or potassium-based (potassium hydroxide and/or potassium silicate) activators [12].

Extensive research has examined the various factors influencing geopolymerisation, with particular emphasis on raw material composition, alkali activator, and curing conditions [13]. Among these, the curing regime plays a particularly critical role in determining the final properties of geopolymers. Typically, either ambient curing or heat curing methods are employed [14]. The strength development of low-calcium geopolymers is slow under normal ambient temperature. Heat curing has been widely reported to enhance early-age strength development due to accelerated geopolymerisation reactions; however, prolonged or excessive heat exposure may lead to internal moisture loss and shrinkage cracking [15]. Balun and Karataş [2] reported that alkali-activated composites prepared with 80% pumice and 20% OPC achieved compressive strengths of up to 93.5 MPa when cured at 100 °C for 72 h, whereas geopolymers prepared entirely from pumice (100%) showed lower strengths. Other studies [10,16,17] also highlighted that heat curing at 60-80 °C for specific durations optimised the mechanical performance of geopolymer systems, although excessive curing temperatures or durations could lead to moisture loss and shrinkage cracking, ultimately reducing strength. Despite these advancements, recent studies have emphasised that curing at moderate temperatures (such as 60 °C) offers a balance between strength development and durability [15,18,19]. However, a limited number of studies have focused on geopolymer curing under high ambient temperature conditions (around 40–50 °C until testing), which are typical in hot climate regions such as Egypt, Iraq, and many African countries. For example, maximum daily temperatures during July and August in Northern Iraq typically range between 39 and 43 °C and may approach 50 °C in extreme cases [20]. This highlights the need for practical curing strategies adapted to on-site conditions, rather than conventional heat curing. Addressing this gap is critical, as hot weather conditions necessitate practical curing strategies that differ from traditional heat curing methods and can significantly influence the long-term performance of geopolymer materials.

In this regard, Rashad and Essa [21] investigated the incorporation of ceramic waste powder into alkali-activated slag pastes cured under a high ambient temperature of 45 °C, demonstrating that early age strength was significantly enhanced due to accelerated slag and ceramic waste powder dissolution, although slight reductions in long term strength were observed. Similarly, Morsy et al. [22] developed eco-friendly lime–pozzolan binders in-

corporating fly ash and ceramic waste powder and showed that high-ambient-temperature curing (50 °C) not only improved early strength development but also contributed to a denser microstructure and reduced water absorption. These studies highlight the potential of high-ambient-temperature curing as a sustainable approach of alkali activated materials in hot climates. However, while these investigations confirm the viability of high ambient curing, its effectiveness has rarely been examined in direct comparison with ambient and heat curing regimes, leaving a gap in understanding the relative performance and long-term implications of different curing strategies.

Fly ash, a by-product of coal combustion, is widely available and has a high aluminosilicate content, making it a well-established geopolymer precursor [19,23]. Meanwhile, pumice, a naturally occurring volcanic material rich in silica and alumina, offers an alternative sustainable resource, particularly in volcanic regions [24]. However, pumice-based geopolymer (PMGP) generally exhibits lower mechanical performance compared to fly ash-based geopolymer (FAGP). Recent studies [10,25] have shown that the addition of metakaolin can significantly enhance the reactivity and mechanical strength of pumice-based geopolymers by increasing their alumina content and promoting more efficient geopolymerisation.

Therefore, the primary novelty of this study lies in curing the geopolymer samples at a high ambient temperature of 45 °C until the testing day, aiming to simulate practical hot weather curing conditions commonly encountered in countries with high climatic temperatures. This approach provides a realistic application model rather than relying solely on conventional heat-curing methods. Following this, the study compares the mechanical performance of samples cured at 25 °C (ambient curing), 45 °C (high ambient curing), and 75 °C (heat curing) in order to assess whether curing under high ambient temperatures can serve as a lower-energy and more climate-adapted alternative to heat curing. Moreover, the performance of fly ash-based and pumice + metakaolin-based geopolymers is systematically evaluated under high ambient curing conditions, enabling a direct comparison of the efficiency of artificial (fly ash) and natural (pumice) pozzolanic systems under realistic hot weather curing environments.

In order to investigate the effectiveness of high-ambient-temperature curing, FAGP and PMGP mortar samples were produced and subjected to three curing regimes, which are ambient temperature, high ambient temperature, and heat curing. The setting times of geopolymer pastes were determined under different curing regimes. Physical tests were carried out to determine density, water absorption, and sorptivity. Compressive strength was measured at 3, 7, 28, and 90 days to observe strength development over time. Durability was evaluated based on resistance to water, freeze–thaw cycles, and exposure to sulphuric and hydrochloric acid. Additionally, Fourier Transform Infrared Spectroscopy (FTIR), X-ray Diffraction (XRD), and Mercury Intrusion Porosimetry (MIP) analyses were used to examine chemical bonds, mineral content, and pore structure. These comprehensive tests were conducted to gain deeper insights into the mechanical and durability performance of the developed geopolymer systems. The outcome of the study is expected to facilitate the development of PMGP and FAGP systems that are better adapted to practical hot curing conditions, providing sustainable alternatives for regions with hot climate conditions.

2. Experimental Programme

2.1. Materials

The pumice used in this study was sourced from Mount Küçük Ağrı (Little Ararat), located in Iğdır, Türkiye. The coarse pumice was ground into a fine powder using a laboratory-scale ball mill equipped with two tubes of 6 L and 9 L capacity, operated simultaneously. Prior to milling, the pumice was oven-dried at 105 °C for 24 h. The grinding was carried out in dry mode, with a rotational speed of 115 rpm, a ball-to-powder weight

ratio of 10:1, and a milling duration of 3 h. Given that pumice and similar natural pozzolans generally exhibit low reactivity, it is often recommended that reactive aluminosilicate materials be partially substituted for pumice to enhance the overall reactivity [26,27]. Therefore, 10 wt% of the pumice was replaced with metakaolin to produce the PMGP mortars. The metakaolin content was limited to 10% in order to maximise the proportion of pumice in the PMGP mixtures. The metakaolin was supplied by GÜNKEM GÜNDÜZ Chemical Substances Industry and Trade Co., Ltd. (Istanbul, Turkey). The fly ash was obtained from the Sugözü Thermal Power Plant (Adana, Turkey).

The chemical compositions of the powder binders, as determined by XRF analysis, are presented in Table 1. As can be seen from Table 1, the SiO_2/Al_2O_3 ratio of the pumice is greater than 5 (Si/Al > 2.5). In other words, the aluminium content of the pumice is relatively low. Aluminium is essential for the bonding of silicon tetrahedra, and its deficiency limits condensation reactions, thereby hindering the adequate formation of geopolymeric gels due to the presence of unreacted silicon [28]. Therefore, in this study, metakaolin was partially used as a replacement for pumice to provide an additional source of aluminium.

Table 1. Chemical compositions of powder binders (wt%).

Powder Binder	CaO	SiO_2	Al_2O_3	Fe_2O_3	MgO	Na_2O	K_2O	SO_3	LOI
Pumice	3.56	67.49	13.07	3.98	0.69	2.63	2.36	0.18	3.69
Metakaolin	0.38	53.29	43.18	0.62	0.22	0.34	0.25	0.16	0.80
Fly ash	3.75	55.98	21.19	6.94	2.45	1.91	2.42	0.42	2.14

The particle size distributions of the powder binders, determined using laser particle size distribution (LPSD), are presented in Figure 1, while some of their key characteristics are given in Table 2.

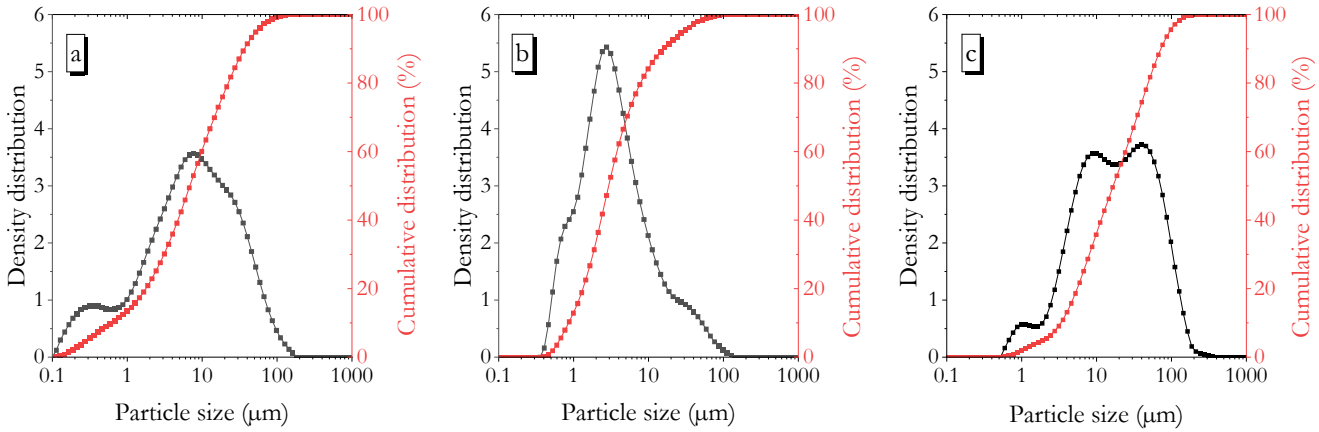

Figure 1. Particle size distributions of pumice powder (**a**), metakaolin (**b**), and fly ash (**c**).

Table 2. Summary of the characteristics of the powder binders: results of LPSD, Blaine surface area, specific gravity, and strength activity index.

Powder Binder	D_{10} (μm)	D_{50} (μm)	D_{90} (μm)	Surface Area of LPSD (cm^2/g)	Blaine Specific Surface Area (cm^2/g)	Specific Gravity	Strength Activity Index (28-Day. %)
Pumice	0.70	8.04	42.0	63,550	4980	2.67	74.2
Metakaolin	0.97	3.34	18.0	25,740	-	2.60	123.0
Fly ash	3.87	19.00	82.10	7220	3004	2.34	92.6

The scanning electron microscope (SEM) micrographs of the powder binders are presented in Figure 2. It is shown that the pumice particles are irregularly shaped and angular due to the grinding process. The metakaolin particles are predominantly small in size, while the fly ash particles mostly exhibit a smooth, spherical morphology.

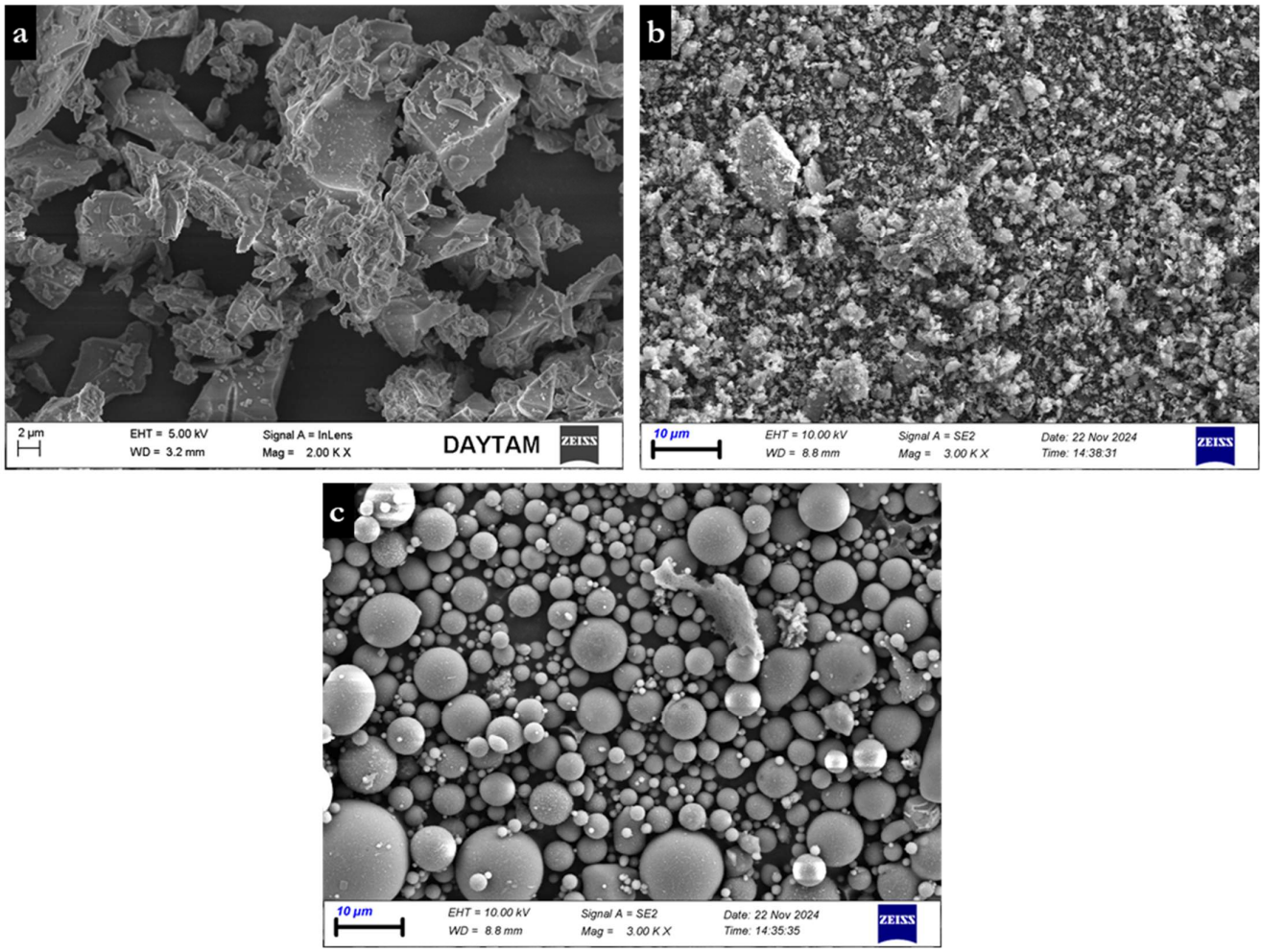

Figure 2. SEM micrographs of pumice powder (**a**), metakaolin (**b**), and fly ash (**c**).

Figure 3a–c shows the raw XRD patterns of pumice, metakaolin, and fly ash, respectively. For pumice, the XRD pattern shows a broad amorphous hump within the 2θ range of 20–30°, which is characteristic of its vitreous nature and high silica content. A few minor sharp peaks are also present, which can be attributed to trace amounts of quartz and albite in the material (Figure 3a). The XRD pattern of metakaolin is notably lacking in distinct crystalline peaks (Figure 3b). A broad hump in the 2θ range of 15–30° reflects its highly amorphous structure, resulting from the dehydroxylation of kaolinite upon calcination. A minor peak near 2θ = 26° suggests the presence of residual quartz impurities in the raw material. The XRD pattern of metakaolin also aligns well with its high strength activity index (123.0%), as presented in Table 2. Figure 3c shows the XRD pattern of the fly ash sample, which displays a broad hump reflecting a predominantly amorphous structure. In addition, several sharp peaks are observed, which are associated with the presence of quartz and mullite. Despite the existence of these crystalline phases, the overall pattern is dominated by an amorphous phase, indicating that the fly ash has high pozzolanic potential.

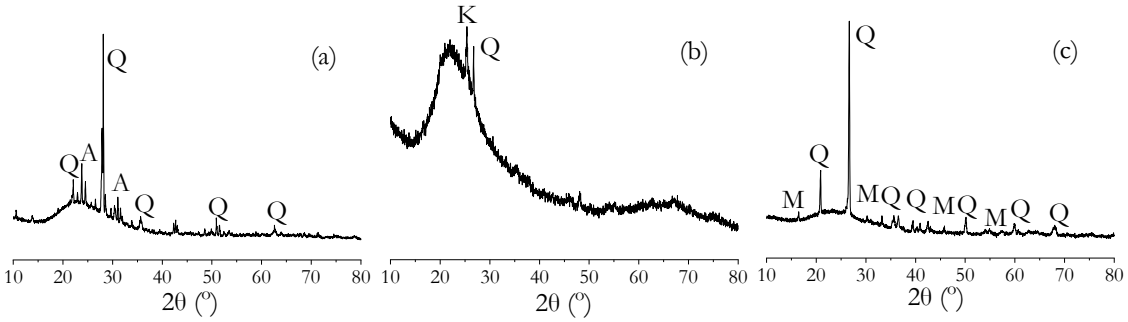

Figure 3. XRD patterns of pumice (**a**), metakaolin (**b**), fly ash (**c**).

An alkaline solution composed of a mixture of sodium hydroxide (NaOH, 98% purity) and sodium silicate (Na_2SiO_3) was used as the activator. The NaOH solution used in the alkaline mixture had a concentration of 10 M. The sodium silicate solution used in the alkaline mixture had an SiO_2/Na_2O weight ratio of 2.04 and a SiO_2 content of 24.50%.

Locally sourced river sand with a specific gravity of 2.73 was used as the fine aggregate in the production of the geopolymer mortars. After washing and oven-drying, the sand was sieved using a standard set, and the fractions were recombined to match the gradation of standard sand according to TS EN 196-1 [29], with a maximum particle size of 2.00 mm. The combined fractions corresponded to 7%, 33%, 67%, 87%, and 99% retained on the 1.60 mm, 1.00 mm, 0.50 mm, 0.16 mm, and 0.08 mm sieves, respectively.

The sulphuric acid (H_2SO_4) and hydrochloric acid (HCl) solutions were obtained from SIGMA-ALDRICH. These acid solutions, which originally had concentrations of 37%, were diluted with deionised water to obtain final concentrations of 5% each.

2.2. Sample Preparation

The geopolymer mortar samples were produced using two different mixtures. The first mixture was a pumice-metakaolin-based geopolymer (PMGP) mortar, in which pumice (90 wt%) and metakaolin (10 wt%) were used as the aluminosilicate sources. The second mixture was a fly ash-based geopolymer (FAGP) mortar, where fly ash was used as the aluminosilicate source. In both mixtures, the weight ratio of Na_2SiO_3 solution to NaOH solution in the alkaline activator was 2.5 [30], and the sand-to-powder binder ratio was 3.0. The alkaline activator, consisting of NaOH and Na_2SiO_3, to powder binder ratio was 0.68 for the PMGP mixture and 0.45 for the FAGP mixture (Table 3). For the PMGP mixture, the powder binder refers to the total mass of pumice and metakaolin, while for the FAGP mixture, it refers to the mass of fly ash. These ratios were determined primarily to ensure adequate workability, and the comparisons in this study should be interpreted as practical, as-mixed evaluations at equivalent workability, rather than direct volume-based comparisons. The lower requirement in the FAGP mixture is attributed to the spherical shape and smooth surface of fly ash particles (Figure 2c), which reduce water demand. In contrast, the higher ratio in the PMGP mixture is related to the irregular, porous structure of pumice particles (Figure 2a) and the very fine particle size of metakaolin (Figure 1b), both of which increase the specific surface area that must be wetted.

Table 3. Mix proportions of geopolymer mortars (g).

Mix Id	NaOH	Na_2SiO_3	Pumice	Metakaolin	Fly Ash	Sand
PMGP	87.4	218.6	405	45	-	1350
FAGP	57.9	144.6	-	-	450	1350

The mixing of the geopolymer mortars was carried out using a cement mixer. Initially, the solids consisting of the powder binder and sand were mixed for 1 min at 62 rpm, followed by the addition of the pre-prepared alkaline activator solution, which was then mixed further—first for 1 min at 62 rpm and then for 1 min at 125 rpm. The prepared geopolymer mortars were then cast into plastic cube moulds with dimensions of 40 mm × 40 mm × 40 mm. After casting, the specimens were placed in waterproof bags and immediately transferred to their designated curing conditions.

2.3. Curing

The geopolymer mortar samples were cured under three different conditions: (i) ambient curing, (ii) high ambient curing, and (iii) heat curing. To evaluate the effectiveness of high ambient curing in geopolymers, both ambient temperature curing commonly used in the literature and heat curing were also applied. For ambient temperature curing, the laboratory temperature (25 °C), which is widely used in previous studies, was selected, while for heat curing, a temperature of 75 °C was chosen, as it is recommended for geopolymer binders synthesised from pumice and fly ash [31,32]. However, when natural pozzolans such as pumice are used, the heat-curing requirement of geopolymer binders increases to some extent. Therefore, for the PMGP mixture, an additional curing at 90 °C for 24 h was applied following the initial 24 h curing at 75 °C. The curing regimes applied to the geopolymer mortars and the corresponding sample IDs are presented in Table 4.

Table 4. Curing regimes applied to the geopolymer mortars and corresponding sample IDs.

Sample ID	Curing Condition
PM-25	Cured at ambient laboratory conditions until the day of testing.
PM-45	Cured at 45 °C continuously until the day of testing.
PM-75	Initially cured at 75 °C for 24 h, followed by 90 °C for 24 h, and then kept at ambient laboratory conditions until testing.
FA-25	Cured at ambient laboratory conditions until the day of testing.
FA-45	Cured at 45 °C continuously until the day of testing.
FA-75	Initially cured at 75 °C for 24 h, then kept at ambient laboratory conditions until the day of testing.

Specimens subjected to high ambient curing and heat curing were demoulded after 1 day, whereas those cured at ambient temperature were demoulded after 3 days due to their slower setting. High-ambient-temperature curing and heat curing were carried out in a laboratory oven, with the specimens kept in waterproof bags during the process.

2.4. Experimental Methods

The initial and final setting times of the geopolymer pastes were determined using a Vicat apparatus in accordance with the relevant standard, TS EN 196-3 [33].

The water absorption and bulk density of the geopolymer mortar specimens were determined on 28-day samples in accordance with TS EN 1015-10/A1 [34]. The sorption coefficients of the geopolymer mortar samples were evaluated following the procedures outlined in TS EN 13057 [35]. Prior to testing, the specimens were conditioned at 38 °C for seven days until a constant mass was achieved, as required by the standard. Subsequently, each sample was placed on supports within a shallow tray containing water, ensuring an immersion depth of (4 ± 1) mm on their bottom surface (Figure 4). Mass measurements were recorded at predetermined time intervals of 12 min, 30 min, 1 h, 2 h, 4 h, and 24 h. The capillary absorption per unit surface area (i) was determined by dividing the increase in mass (kg) by the exposed surface area (m^2) for each recorded time. The (i) values were graphed as a function of the square root of the immersion time (h). The slope obtained from this graph was reported as the sorption coefficient (S), expressed in units of [$kg/(m^2 \cdot h^{0.5})$].

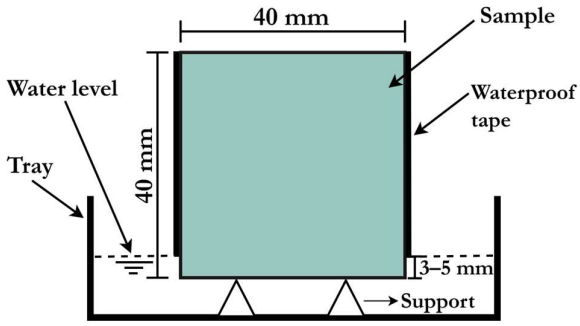

Figure 4. Experimental arrangement used to determine the sorption coefficient of geopolymer mortars.

The compressive strengths of the geopolymer mortar specimens were determined at 3, 7, 28, and 90 days in accordance with TS EN 196-1 [29], using a cement compression testing machine.

Rees et al. [36] define geopolymers as materials synthesised by mixing a source of alkali metal, silica, and alumina in a highly alkaline solution, which are capable of retaining their hardness after solidification in water. Therefore, the resistance of a geopolymer binder to water is considered one of the most critical indicators in determining its suitability as a construction material [37]. To evaluate the effectiveness of high ambient curing, a water resistance test was conducted. Water resistance was assessed by immersing 28-day specimens in a large tank filled with water for 72 h, followed by measuring their compressive strength in a saturated surface-dry condition. The compressive strength obtained under this condition is defined as the "wet strength". The water resistance of the geopolymer mortars was then calculated as the ratio of the wet strength to the dry strength.

Freeze–thaw tests on the geopolymer mortar samples were carried out in accordance with ASTM C666 Procedure A [38] using a freeze–thaw chamber. The samples, placed in containers filled with water, were cooled down to −18 °C over a period of 120 min and held at this temperature for 30 min. Afterwards, their temperature was increased to +4 °C over the next 120 min and maintained at this level for an additional 30 min. In this way, each freeze–thaw cycle lasted a total of 5 h, adhering to the temperature and duration conditions defined in ASTM C666 Procedure A. Following 25 such cycles, the compressive strengths of the FGP concretes were determined under saturated surface-dry conditions.

To determine the acid resistance of the geopolymer mortars, 28-day specimens were first immersed in water for 24 h to reach saturation. The samples were then immersed separately in 5% concentration solutions of H_2SO_4 and HCl for a period of 75 days. At the end of this period, the residual compressive strengths of the specimens were determined under saturated surface-dry conditions.

Three specimens were tested for each data point in the physical properties, compressive strength (at 3, 7, 28, and 90 days), and durability tests (water resistance, freeze–thaw, sulphuric acid, and hydrochloric acid).

The particle size distributions of the raw fly ash samples were determined using a laser diffraction particle size analyser (Malvern Mastersizer 3000, Malvern Panalytical Ltd., Malvern, UK). The chemical composition of the aluminosilicate sources was assessed by means of a wavelength-dispersive X-ray fluorescence spectrometer (Panalytical Axios Advanced, Malvern Panalytical Ltd., Almelo, The Netherlands).

In order to examine the molecular bonding structure of the geopolymer binders under different curing conditions, a Fourier Transform Infrared (FTIR) spectrometer (Agilent Cary 630, Agilent Technologies, USA) was utilised. The device operated within a wavelength range of 4000 to 650 cm^{-1}.

The mineralogical composition of the geopolymer binders under different curing conditions was analysed using an X-ray diffractometer (TD-3500, Tongda Instrument,

Dandong, China). Measurements were carried out over a 2θ range of 10° to 80°, with a step size of 0.02°.

The pore structure of the geopolymer samples was characterised by mercury intrusion porosimetry (MIP), conducted with a Quantachrome Pore Master 60 (Anton Paar QuantaTec Inc., Boynton Beach, FL, USA). This technique enabled the identification of pore size distribution within the range of 4 nm to 10 μm by applying pressures up to 55,000 psi in a high-pressure chamber.

For FTIR, XRD, and MIP analyses, geopolymer pastes were used instead of mortars. These pastes were prepared to have the same consistency as the corresponding mortars, with an alkali activator to binder ratio of 0.53 for PMGP and 0.33 for FAGP. The prepared paste samples were subjected to the same three curing regimes as the mortars. At 7, 28, and 90 days, samples were removed from the curing environments indicated in Table 4. They were first crushed using a jaw crusher and then sieved through a 0.5 mm sieve. The fraction passing through the sieve was ground in a ring mill to obtain a powder smaller than 63 μm, which was then used for FTIR and XRD analyses. The coarse fraction retained on the 0.5 mm sieve was used for MIP analysis (only for the 90-day samples). All analyses were conducted within two days after sample removal from the curing conditions.

3. Results and Discussion

3.1. Setting Times

The mixing, transportation, placement, compaction, and surface finishing processes of fresh concrete are carried out within its handling period. The setting time is a crucial parameter that governs the duration during which fresh concrete remains workable. If the setting time is too short, it leads to rapid stiffening, thereby hindering the proper handling of the fresh concrete. Conversely, excessively long setting (gaining rigidity) and hardening (gaining strength) times extend the mould removal period in construction, ultimately delaying the overall project and increasing costs [39].

Therefore, it is essential to ensure an appropriate setting time to enable the proper handling of fresh concrete. Experimentally determined initial setting time approximately represents the point at which fresh concrete can no longer be adequately mixed, placed, or compacted, whereas the final setting time corresponds to the point when significant strength development begins [40]. The initial and final setting times of the geopolymer pastes are presented in Figure 5. It is seen that both geopolymer pastes exhibited initial and final setting times exceeding 24 h (1440 min) at ambient temperature. It has also been reported in other studies that the setting time of FAGPs produced with low-calcium fly ash exceeds 24 h [41,42]. On the other hand, the setting time of geopolymers produced with low-reactivity materials such as natural pozzolan can extend to several days under ambient conditions [27,43]. In this study, it was observed that replacing 10% by weight of pumice with metakaolin, a reactive material, significantly reduced the setting time of PMGP. The slow setting and hardening of low-calcium geopolymers under ambient conditions limit their applicability in in situ concrete casting.

The setting of low-calcium geopolymers can be accelerated by incorporating calcium-rich sources or applying heat curing [44,45]. Heat curing facilitates the dissolution of Si and Al species from the aluminosilicate material, thereby promoting the polycondensation process [27,46]. This results in an accelerated solidification process of the geopolymer. Similarly, in this study, the application of heat curing at 75 °C reduced the initial and final setting times of PMGP to 55 and 80 min, respectively, while for FAGP, these values shifted to 50 and 90 min. It can be stated that heat curing, which is suitable for precast concrete structural elements, provides an appropriate period for the solidification of fresh geopolymer concrete once the handling process is completed.

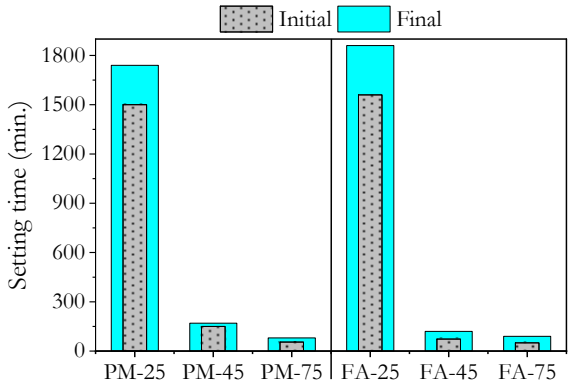

Figure 5. Initial and final setting times of geopolymer pastes conditioned at different curing regimes.

When curing was carried out at a high ambient temperature (45 °C), representing the environmental conditions of hot regions, the setting times of the geopolymers were significantly lower than those at ambient temperature and were comparable to those under heat curing. At this elevated ambient temperature, the initial and final setting times of PMGP were 150 and 170 min, respectively, while for FAGP, these values were 73 and 120 min. According to ASTM C150 [16], the initial setting time of OPC concrete should not be shorter than 45 min, and the final setting time should not exceed 375 min. Both geopolymer binders satisfy these requirements. Nevertheless, the initial setting time of FAGP is relatively short. Therefore, when FAGP concrete is used in regions where daily temperatures exceed 45 °C, detailed planning will be required during the handling process to prevent potential complications.

3.2. Physical Properties

Figure 6 presents the water absorption and apparent porosity of the geopolymer mortars under different curing regimes. As can be seen, the water absorption of PMGP mortar samples ranges from 4.39% to 6.73%, while for FAGP samples it ranges from 3.18% to 5.11%. For both mixtures, the samples subjected to heat curing exhibit higher water absorption than those cured at ambient and high ambient temperatures. The apparent porosity of PMGP mortar ranges from 9.5% to 14.1%, whereas for FAGP mortar it ranges from 7.0% to 11.0%. Water absorption tends to be closely related to apparent porosity [7]. Therefore, there is a strong correlation between water absorption and apparent porosity. High temperatures during the curing process cause evaporation of water, leading to increased porosity. Consequently, the water absorption of geopolymer mortar samples cured at 75 °C is higher than that of those cured at ambient temperature. Similarly, Yılmaz et al. [15] reported that low-calcium fly ash-based geopolymer samples cured at 80 °C generally exhibited lower water absorption compared to those cured at lower temperatures. In contrast, Djobo et al. [47] found that volcanic ash-based geopolymer mortar samples cured at 80 °C absorbed less water than those cured at 27 °C. However, the water absorption values reported in the latter study were relatively close to each other. The water absorption of PMGP and FAGP samples cured at elevated ambient temperature were 4.39% and 3.18%, respectively. For both geopolymer mixtures, the samples cured at high ambient temperature showed lower water absorption than those cured at ambient temperature and by heat curing. This indicates that samples cured at high ambient temperature exhibit relatively fewer harmful pores induced by heat curing [48]. Furthermore, the application of high ambient temperature over 28 days resulted in the formation of more geopolymerisation products in these samples compared to those cured at ambient temperature, leading to a greater filling of capillary voids.

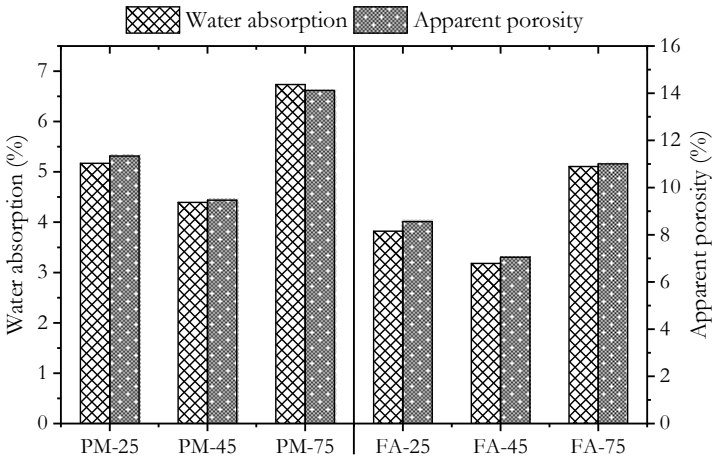

Figure 6. Water absorption and apparent porosity of the geopolymer mortars.

Figure 7 presents the bulk density and apparent density of geopolymer mortars under different curing profiles. For PMGP mortar, the bulk density ranges between 2096 and 2193 kg/m^3, whereas for FAGP mortar, it ranges between 2155 and 2241 kg/m^3. The apparent density of PMGP mortar varies from 2380 to 2474 kg/m^3, while for FAGP mortar it ranges from 2384 to 2450 kg/m^3. When each curing profile is considered individually, the bulk density of FAGP mortar is higher than that of PMGP mortar. This can be explained by the fact that, for a given volume, FAGP mortar contains relatively more geopolymer paste and less aggregate compared to PMGP mortar (Table 3). Since both the alkaline activator and the powder binder forming the paste have lower specific gravities than the aggregate, the bulk density of FAGP mortar becomes higher than that of PMGP mortar.

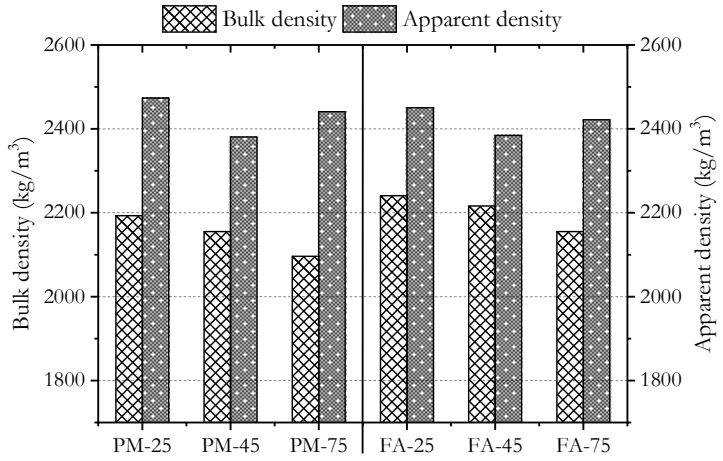

Figure 7. Bulk density and apparent density of the geopolymer mortars.

For both geopolymer mixtures, an increase in curing temperature results in a decrease in the bulk density of the sample (Figure 7). However, as can also be seen from the same figure, the apparent density is lowest in samples cured at high ambient temperatures and highest in those cured at ambient temperature. Bulk density reflects the presence of both open and closed pores within the sample, whereas apparent density accounts only for the closed pores, excluding the open ones. Therefore, when bulk density and apparent density are considered together, it can be concluded that samples cured at high ambient temperatures contain a greater proportion of closed pores compared to those cured under the other curing conditions. In addition, samples cured at ambient temperature appear to have the lowest proportion of closed pores.

Figure 8 presents the sorptivity test results of the geopolymer mortars. As shown in Figure 8, for the FA-45 and FA-75 samples, the amount of water absorbed per unit area increases approximately linearly with the square root of time, indicating that water absorption is proportional to the square root of the testing time. For these two samples, the slope of the curve in the graph is considered the sorptivity coefficient. In contrast, for the other samples, since they approach near saturation before the end of the test duration, the slope of the initial linear portion of the graph is taken as the sorptivity coefficient, in accordance with the relevant standard [35]. The sorptivity coefficients obtained in this manner are given in Figure 8b. For PMGP mortar, the sorptivity coefficient decreases with increasing curing temperature; however, this reduction is limited. Although the sorptivity coefficients of these samples are relatively similar, the capillary water absorption rate of the sample cured at ambient temperature is noticeably higher than that of the other two. Therefore, for mortars and concretes with high porosity, such as PMGP, taking measurements at shorter time intervals than those specified in the relevant standard [35] may be a more appropriate method for comparison.

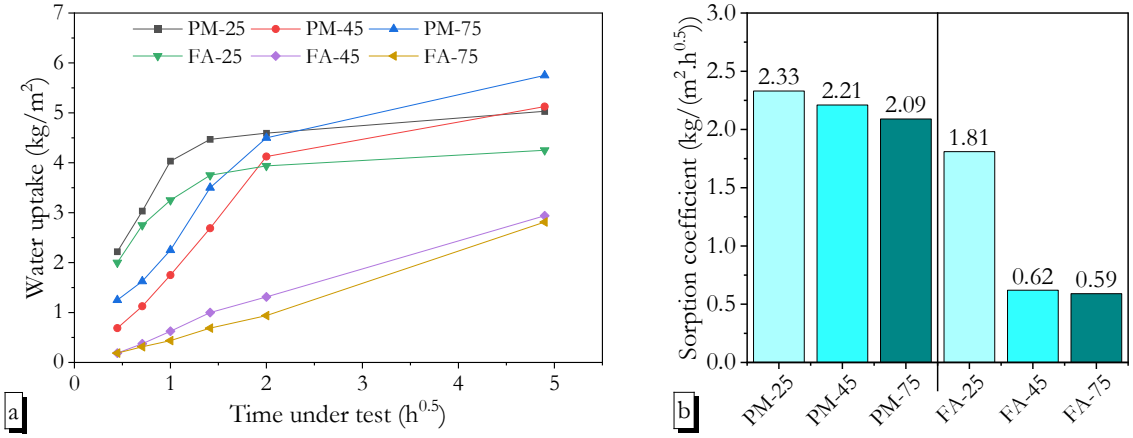

Figure 8. Sorptivity test results: variation in water absorption per unit surface area with time (**a**), sorptivity coefficients of the samples (**b**).

According to TS EN 1504-3 [49], the sorption coefficient limit for OPC mortars is specified as 0.5 kg/(m^2·h$^{0.5}$). None of the samples in this study met this requirement. A key reason for the high permeability of both PMGP and FAGP mortars is that their binder phase predominantly consists of N-A-S-H gel. In calcium-free geopolymerisation, water acts mainly as a reaction medium, transporting alkali species necessary for the reaction, as well as cations released from the binder surface and newly formed ionic groups in the early stages. However, it does not directly participate in the formation of geopolymerisation products [50]. The resulting N-A-S-H gel contains a low amount of bound water, and to reflect this, some studies refer to it as N-A-S-(H) or simply N-A-S gel [51,52]. Upon completion of geopolymerisation, the evaporation of unbound water leaves behind harmful pores within the matrix. Consequently, the total pore volume and permeability of low-calcium geopolymers are significantly higher than those of OPC- or alkali-activated slag-based materials [53].

The high sorptivity coefficients observed in all PMGP mortars and in FAGP samples cured at ambient temperature can be attributed to the limited extent of geopolymerisation in these mixes. Due to the low reactivity of pumice, PMGP mortar was unable to form sufficient amounts of geopolymer gel under any of the three curing profiles, resulting in inadequate filling of capillary pores [26]. Similarly, as fly ash has moderate reactivity, it could not achieve sufficient geopolymerisation under ambient curing conditions. One of the important reasons why PMGP mortars exhibit higher sorptivity coefficients than FAGP

mortars is their larger paste phase content. Since the paste is relatively more permeable, the higher paste content in PMGP mortars leads to greater capillary water absorption compared to FAGP mortars.

An increase in curing temperature led to a decrease in the sorptivity coefficient for both geopolymer mortars. Although the water absorption of heat-cured samples was the highest for both mixes, their sorptivity coefficients were the lowest. This can be explained by differences in pore structure. In PMGP and FAGP, the pore structure of the samples was primarily influenced by two factors. The first was heat curing, which caused water to evaporate from the samples, leaving behind large voids. As a result, heat-cured samples exhibited the highest apparent porosity. The second factor was the extent of geopolymerisation, which contributed to the filling of capillary pores with geopolymer gel and increased the tortuosity of pore channels. In heat-cured samples, although the apparent porosity was high, the more intricate and less connected pore network hindered water movement, thereby reducing the sorptivity coefficient. In contrast, the pore structure of ambient-cured samples exhibited the opposite characteristics. Meanwhile, samples cured at high ambient temperatures showed lower apparent porosity and, similar to heat-cured samples, a capillary structure with reduced connectivity and a greater number of closed pores.

3.3. Compressive Strength Development

Geopolymerisation involves the dissolution of amorphous aluminosilicate materials in a high-pH alkaline solution, the formation of Si and Al monomers from the dissolved species, and the subsequent polymerisation of these monomers into a three-dimensional network that hardens over time. The curing temperature plays a key role in the dissolution of the aluminosilicate source. A higher curing temperature speeds up this dissolution, allowing the geopolymerisation process to take place more quickly [54]. This accelerates the solidification process and shortens the setting time (Figure 5). In addition, faster geopolymerisation at higher temperatures leads to higher early strength. This is clearly illustrated in Figure 9, presenting the compressive strength development over 90 days along with the rate of strength gain. At lower curing temperatures, the dissolution of the aluminosilicate source occurs at a reduced rate and to a limited extent [55]. As a result, the geopolymerisation process proceeds at a slower rate, leading to longer setting times and lower rates of strength gain. Furthermore, when low-reactivity precursors such as pumice are used in geopolymer synthesis, the strength development tends to be less pronounced [10,27]. Since fly ash is more reactive than pumice, FAGP shows a significantly faster strength gain than PMGP, especially at early ages (Figure 9b). It should also be noted that, when a specific curing regime is considered, the lower strength of PMGP compared to FAGP is mainly attributed to its higher alkali activator-to-binder ratio (0.68 versus 0.45). As is well known, an increase in the liquid content in mortars and concretes generally results in lower strength and durability.

Due to the limited strength development at low temperatures, the 3-day compressive strengths of PMGP and FAGP mortars cured at ambient temperature were relatively low, measuring 2.0 MPa and 3.4 MPa, respectively. When cured at high ambient temperature, these values increased significantly to 9.3 MPa for PMGP and 40.3 MPa for FAGP. The much greater increase observed in FAGP is attributed to the higher reactivity of fly ash compared to pumice, suggesting that pumice requires higher heat curing demand for effective activation. Notably, when heat curing was applied instead of high ambient curing, the 3-day strength of PMGP showed a marked improvement (from 9.3 MPa to 17.1 MPa), whereas FAGP exhibited only a slight increase (from 40.3 MPa to 43.4 MPa). These results indicate that heat curing is more beneficial for early strength gain in PMGP mortars. In

contrast, for FAGP mortars, high ambient curing alone is sufficient to eliminate the need for additional heat curing at early ages.

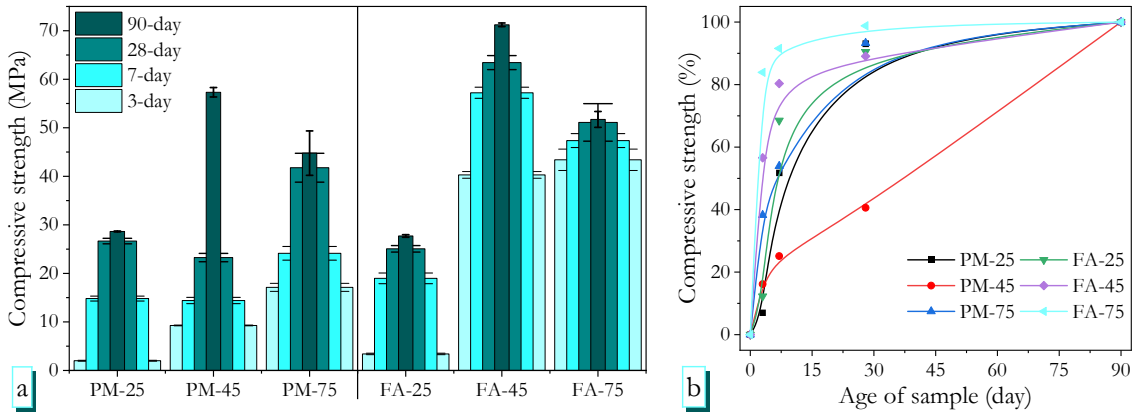

Figure 9. Compressive strength development (**a**) and relative strength gain (**b**) of geopolymer mortars over 90 days.

At the beginning of the mixing process between the powder binder and the alkali activator, the geopolymer paste consists of powder binder particles with voids filled by activator solution in between. As the reactions proceed, the resulting geopolymer gel gradually fills these pores. The degree of pore refinement reduces the permeability of the mortar and contributes to an increase in strength. As shown in Figure 8, increasing the curing temperature enhances the degree of geopolymerisation, leading to lower permeability. This also results in a significant improvement in early-age strength. However, at higher curing temperatures such as 75 °C or 90 °C, the reactions proceed very rapidly, and the gel formed tends to be less homogeneously distributed and more disordered in structure [53,56,57]. As shown in Figure 9a, the standard deviation values of the specimens cured at high temperatures are generally greater than those cured at ambient and high ambient temperatures. This suggests that the less ordered gel produced at high temperatures may lead to localised defects. Therefore, heat curing may not be suitable for long-term strength development [48].

Although an increase in curing temperature accelerates the strength development of geopolymer mortars, the rate of strength gain for PMGP cured at high ambient temperature is lower than that of the specimen cured at ambient conditions. It is seen that the PMGP mortar cured at ambient temperature reaches 51.7% of its 90-day strength within the first 7 days, and 93.1% within 28 days (Figure 9b). In contrast, the strength development of the sample cured at high ambient temperature is more gradual and follows an approximately linear trend over time. This suggests that the dissolution of pumice is limited under ambient conditions, whereas it continues progressively at high ambient temperatures. Moreover, strength losses reported under prolonged exposure to high temperatures such as 75–90 °C [18,58] were not observed under extended high-ambient-temperature curing. The continuous increase in strength of the PMGP mortar under prolonged high ambient curing indicates a gradual increase in geopolymer gel formation and a greater degree of cross-linking within the three-dimensional aluminosilicate network [59]. This behaviour was not observed in the FAGP mortar, which can be attributed to the relatively high reactivity of fly ash. A significant portion of the reactive fly ash particles dissolve within the first 7 days of high-ambient-temperature curing. Indeed, the 7-day strength of the FAGP mortar cured at high ambient temperature is higher than the 90-day strength of the samples cured under heat curing conditions (Figure 9a). This indicates that high ambient curing is highly effective for FAGP mortars, particularly in terms of early-age performance. Therefore, in

hot climate regions, FAGP mortars and concretes can be cast in place without the need for heat curing or calcium-rich additives such as slag. As a result, these materials are expected to find broader application and become both cost-effective and environmentally friendly by eliminating the need for heat curing.

3.4. Water Resistance

According to European (EN) and American (ASTM) standards, the compressive strength of OPC concretes should be tested while the specimens are in a wet or moist condition. Samples tested in the dry state typically exhibit higher compressive strength values. This difference is mainly due to the dilatation effect caused by water adsorbed in the C-S-H gel. It is believed that the adsorbed water trapped between two solid surfaces creates a wedge-like action that pushes them apart. As a result, the compressive strength of a wet OPC concrete sample is generally about 10–15% lower than that of the same sample tested dry [40,60,61]. In contrast, for geopolymer-based materials, the ratio of wet to dry compressive strength—referred to in this study as the water resistance index—shows significant variation. Therefore, water resistance is considered a key test in evaluating the long-term durability of geopolymer binders [36,37].

Figure 10 shows the compressive strengths of PMGP and FAGP mortars in dry and wet conditions under different curing regimes. The figure also shows the water resistance index of the geopolymer mortars. The water resistance indices of the FAGP mortars cured at high ambient temperature and heat curing are 0.90 and 0.87, respectively, which are comparable to those of OPC mortars and concretes. This suggests that these two FAGP mortars possess effective water resistance. However, the FAGP mortar cured at ambient temperature shows a relatively low water resistance index (0.58), indicating that the three-dimensional aluminosilicate network may not have fully developed under the low-temperature curing condition (25 °C).

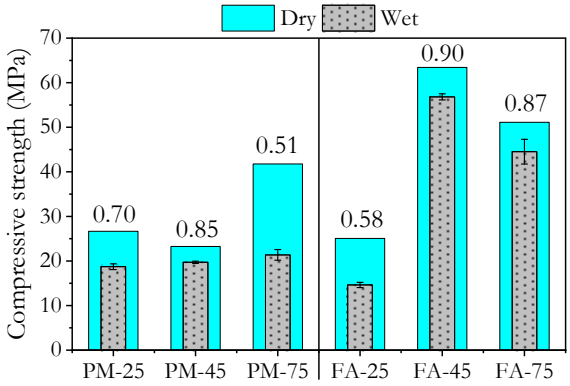

Figure 10. Compressive strengths of geopolymer mortars in dry and wet conditions.

The water resistance index of the PMGP mortar cured at high ambient temperature was 0.85. Although the strength development of this mortar was relatively slow, the high water resistance index suggests the formation of a robust gel structure. Among the PMGP mortars, the heat-cured sample exhibited the highest compressive strength, yet it unexpectedly showed the lowest water resistance index (0.51) among all geopolymer mortars. This indicates the presence of sodium silicate gel in the heat-cured PMGP. In geopolymer systems with high silica content, high temperatures promote the hardening of sodium silicate-based compounds, leading to strength gains. However, these products tend to be less hydrolytically stable, resulting in strength loss upon exposure to water [37,62]. Similarly, in the heat-cured PMGP mortar, the high-temperature regime of 75 °C followed by 90 °C significantly increased strength compared to ambient-cured samples. Nevertheless,

the lack of hydrolytic stability in the sodium silicate gel caused a 48.9% loss in strength when exposed to water.

The ambient-cured PMGP mortar exhibited a water resistance index of 0.70, much higher than that of the ambient-cured FAGP mortar, which had a value of 0.58. This is likely due to the replacement of 10% of pumice with metakaolin in the PMGP mix. Metakaolin, known for its high reactivity, dissolves effectively even at ambient temperatures (25 °C), promoting the formation of a geopolymeric gel. Furthermore, the fine particle size of metakaolin contributes to a filler effect, which helps reduce the impact of water on the binder gel.

3.5. Freeze–Thaw Durability

The compressive strength of the geopolymer mortars after 25 freeze–thaw cycles was measured in the wet state. It is important to compare the post-cycle strength not only with the dry compressive strength but also with the wet strength. Figure 11a,b compare the compressive strengths measured after 25 freeze–thaw cycles with the dry strength and the wet strength, respectively. The PMGP mortar cured at high ambient temperature and the FAGP mortar cured at ambient temperature disintegrated after 25 cycles; thus, their compressive strengths could not be measured. This may be attributed to their initially low strength before exposure to freeze–thaw cycles. The PMGP mortar cured at ambient temperature experienced a strength loss of 48.8% compared to its dry strength and 27.1% compared to its wet strength after freeze–thaw cycles. This reduction may also be linked to its initially low compressive strength.

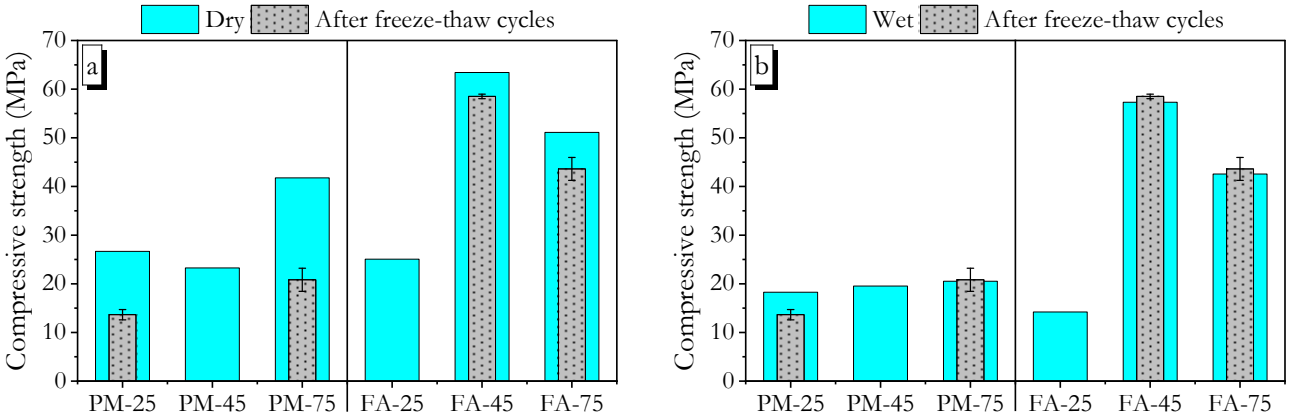

Figure 11. Compressive strengths after 25 freeze–thaw cycles compared with dry (**a**) and wet (**b**) strengths.

The heat-cured PMGP mortar, as well as the FAGP mortars cured at high ambient temperature and by heat curing, showed almost no deterioration after 25 freeze–thaw cycles (Figure 11b). This is because their compressive strengths in the wet state before and after the cycles remained nearly the same. This durability can be attributed to their relatively high initial compressive strengths, which likely enhanced their resistance to freeze–thaw damage. Therefore, it can be concluded that these three geopolymer mortars possess adequate resistance to freeze–thaw action. This also suggests that, in geopolymer systems with similar compositions, a correlation may exist between freeze–thaw resistance and compressive strength [63].

3.6. Acid Resistance

Concrete structures are exposed to various aggressive environmental conditions throughout their service life. Infrastructure elements in contact with sewage pipes, marine environments, or contaminated soil and groundwater are often subjected to sulphuric acid attack, while industrial structures are frequently exposed to hydrochloric acid [64]. Since

resistance to such acids is a key indicator of the durability of construction materials, this study investigates the resistance of the produced geopolymer mortars to sulphuric and hydrochloric acid.

3.6.1. Sulphuric Acid

Figure 12a,b compare the residual compressive strength of the geopolymer mortars after 75 days of immersion in a 5 wt% sulphuric acid (H_2SO_4) solution with their dry and wet strengths, respectively. When compared with the dry strength, the strength losses of PM-25, PM-75, and FA-25 mortars are relatively high: 27.0%, 29.0%, and 35.4%, respectively (Figure 12a). However, these losses are mainly due to the measurements being taken in the wet state, rather than a damaging effect of the acid solution itself. In fact, the compressive strength measured in the wet state after acid exposure is higher than that measured in the wet state before acid exposure (Figure 12b). This suggests that the 75-day immersion in sulphuric acid led to an improvement in strength for these geopolymer mortars. On the other hand, a slight decrease in strength was observed in the FA-45 and FA-75 mortars.

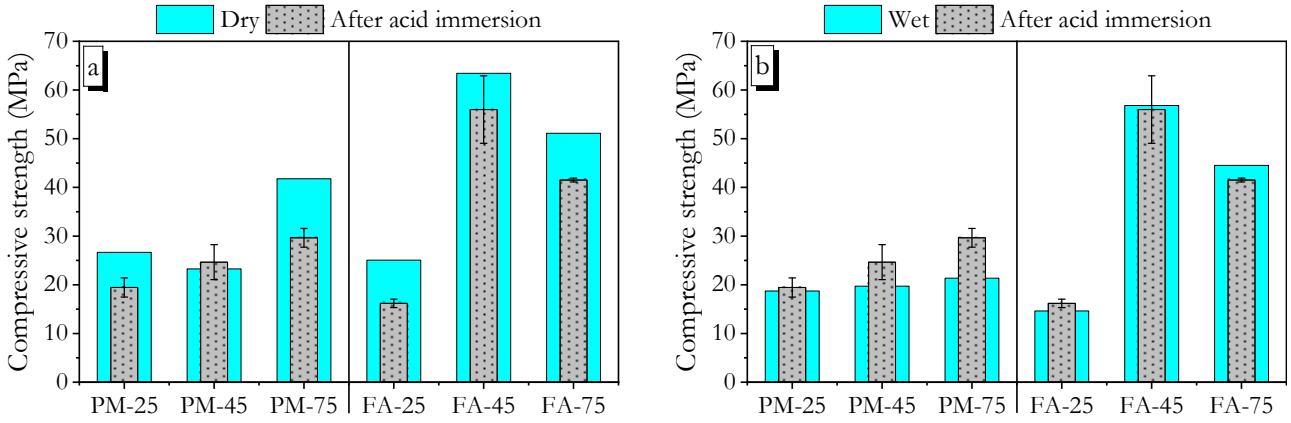

Figure 12. Residual strengths after 75 days in 5% H_2SO_4 compared with dry (**a**) and wet (**b**) strengths.

OPC concretes deteriorate rapidly in 5 wt% sulphuric acid solution and may completely disintegrate or collapse within approximately 120 days [65,66]. In geopolymer systems with high calcium content, calcium reacts with sulphuric acid to form gypsum ($CaSO_4.2H_2O$) [67]. The gypsum precipitates within the pores, causing volumetric expansion, which leads to cracking and, consequently, strength loss in geopolymer mortars and concretes. On the other hand, in low-calcium geopolymer systems, degradation due to sulphuric acid is more limited [26]. Similarly, the low-calcium geopolymer mortars exhibited only minor strength loss under acid exposure, as shown in Figure 12b. This highlights the high stability of the aluminosilicate framework in geopolymers. Furthermore, the fact that some mortars showed higher wet strength after 75 days of acid exposure than before may be attributed to the presence of sodium-rich gels. These gels may interact with sulphuric acid through acid-base reactions, helping to neutralise the acid and thus limiting structural degradation in the gel matrix [47]. In addition, the reaction products formed during acid exposure may fill pores in the geopolymer matrix, further contributing to strength improvement [68].

3.6.2. Hydrochloric Acid

Figure 13a,b compare the residual compressive strength of geopolymer mortars exposed to a 5 wt% hydrochloric acid (HCl) solution for 75 days with their dry strength and wet strength, respectively. The strength losses for PM-25, PM-75, and FA-25 mortars were significant, with corresponding losses of 36.5%, 36.6%, and 32.1% (Figure 13a). However,

similar to the behaviour under sulphuric acid attack, the residual strengths of these mortars were close to their wet strengths (Figure 13b). To further clarify this, Figure 14 presents the compressive strengths of geopolymer mortars after exposure to different aqueous environments, including tap water, sulphuric acid solution, and hydrochloric acid solution.

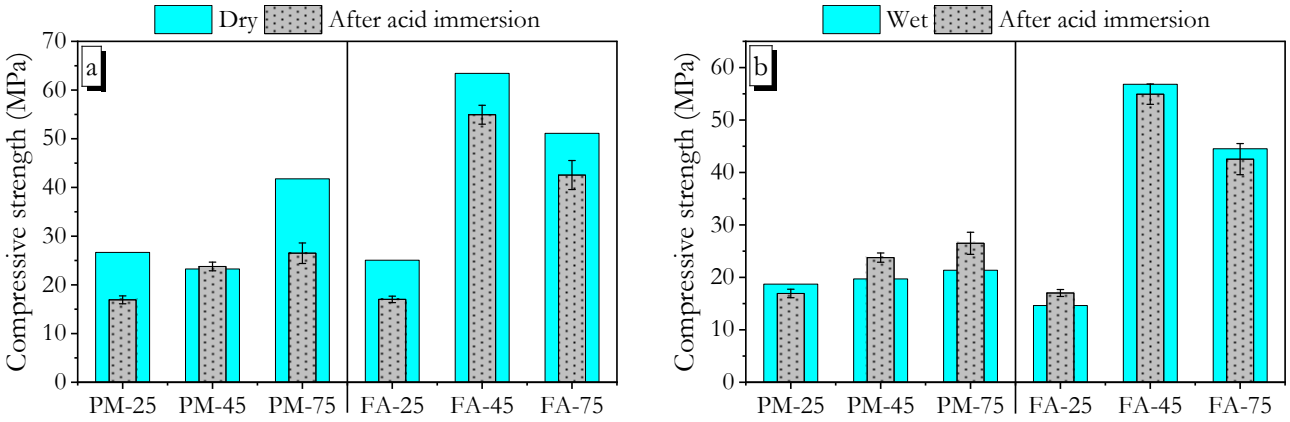

Figure 13. Residual strengths after 75 days in 5% HCl compared with dry (**a**) and wet (**b**) strengths.

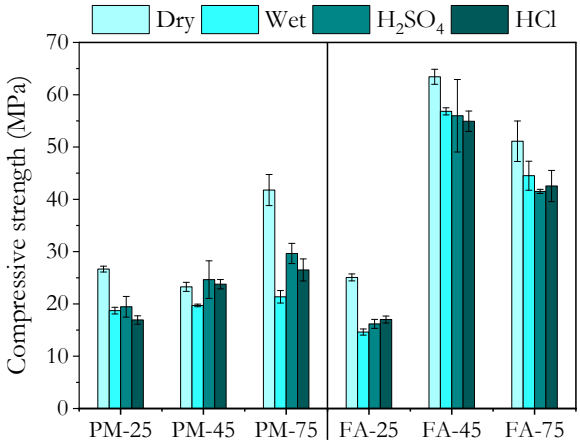

Figure 14. Compressive strengths of geopolymer mortars before exposure (dry) and after exposure to tap water, H_2SO_4, and HCl.

Figure 14 shows that the three aqueous environments do not cause significant differences in the residual compressive strengths of the geopolymer mortars. In other words, the residual compressive strengths of the mortars, which were exposed to different aqueous environments and tested in wet conditions, are quite similar. Similarly, Zhang et al. [69], reported that alkali-activated waste materials kept in pure water, seawater, and an acidic solution exhibited quite similar strength losses. This observation suggests that geopolymers with low calcium content generally show high resistance to acidic environments [26].

For all PMGP mortars cured under different regimes, the residual compressive strength after hydrochloric acid attack was lower than that after sulphuric acid exposure. This may primarily be attributed to the ability of hydrochloric acid to promote aluminium dissolution [64,70]. In the PMGP mixture, 10% of the pumice was replaced with alumina-rich metakaolin, thereby increasing the aluminium content of the mix. As a result, the geopolymeric gel in the PMGP mortars, which contained higher aluminium levels, experienced greater aluminium dissolution under hydrochloric acid, leading to more pronounced strength loss compared to sulphuric acid exposure. In contrast, the FAGP mortars showed relatively similar strength losses under both sulphuric and hydrochloric acid attacks. This may be attributed to the more balanced aluminium content in these mixtures.

As can be clearly seen in Figure 14, the wet-state compressive strengths of the high ambient-cured PMGP, high ambient-cured FAGP, and heat-cured FAGP after exposure to tap water, H_2SO_4, and HCl remained close to their corresponding dry-state strengths. This indicates that these three geopolymer mortars exhibit comparable performance in aqueous environments.

3.7. Chemical Bonding Characterisation by FTIR

The chemical bonding structures of the geopolymer binders were characterised using Fourier Transform Infrared (FTIR) spectroscopy. The FTIR spectra of PMGP and FAGP binders cured under different regimes are shown in Figures 15 and 16, respectively. In geopolymer spectra, the strongest band, referred to as the 'main band', in the 1200–900 cm^{-1} region is associated with the asymmetric stretching vibration of Si-O-T bonds (T: Si or Al) [71,72]. Shifts in the wavenumber of this main band indicate changes in the chemical structure of the geopolymer gel. Figure 15 shows that the main band in the FTIR spectrum of PMGP cured at ambient temperature shifts towards higher wavenumbers over time. This shift indicates that geopolymerisation continues for an extended period under ambient conditions. According to Zhang et al. [48], during the initial stage of geopolymerisation, when the aluminosilicate source dissolves in the alkaline medium, the main FTIR spectra band appears at lower wavenumbers. As polymerisation progresses and silicate and aluminate oligomers form, the band shifts to higher wavenumbers [73]. In this stage, Al-rich gel gradually transforms into Si-rich gel. Since strength development in geopolymers is largely attributed to the formation of Si-rich gel [74], the significant strength gain observed in PMGP cured at ambient temperature (PM-25) over time aligns well with the FTIR findings (Figure 9).

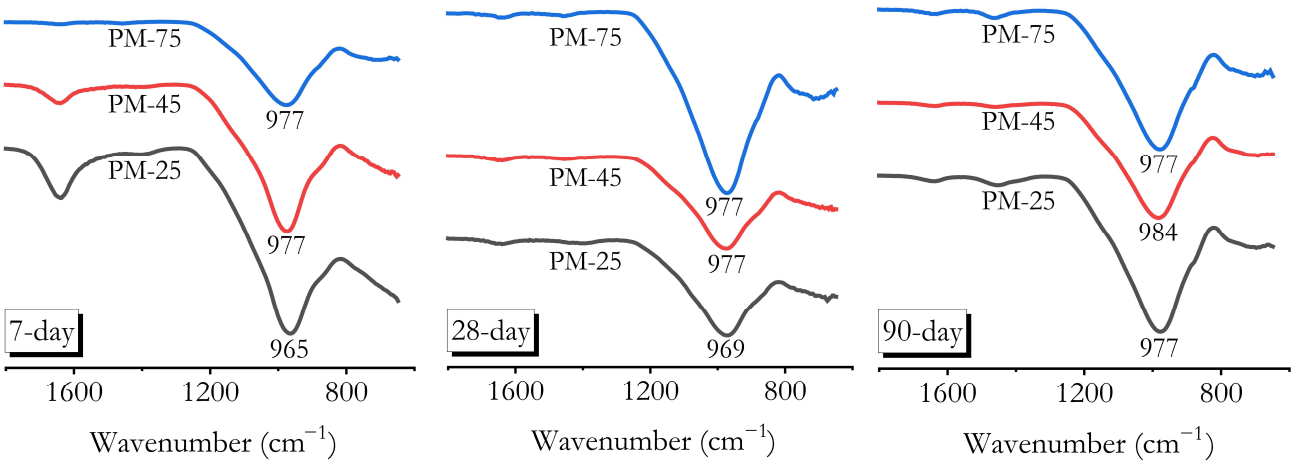

Figure 15. FTIR spectra of 7-, 28-, and 90-day PMGP samples cured under ambient, high ambient, and heat curing conditions.

The main bands of the FTIR spectra of PMGPs at 7 days appear at higher wavenumbers (977 cm^{-1}) for those cured at high ambient temperature and under heat curing, compared to the ones cured at ambient temperature (965 cm^{-1}). Moreover, the main band in the spectra of heat-cured PMGP remains stable over time, indicating that most of the geopolymerisation reactions were completed within the first 7 days. However, the main band in the FTIR spectrum of the PMGP binder cured at high ambient temperature interestingly shifted from 977 cm^{-1} to 984 cm^{-1} between 28 and 90 days. This also clearly explains the significant increase in the compressive strength of the PMGP cured at high ambient temperature (PM-45) between 28 and 90 days (Figure 9a,b). These results suggest that in high-ambient-temperature curing, the dissolution of pumice continues beyond 28 days, enabling further

polymerisation of silicate and aluminate oligomers and the ongoing conversion of Al-rich gel into Si-rich gel. Consequently, a notable strength gain occurs after 28 days.

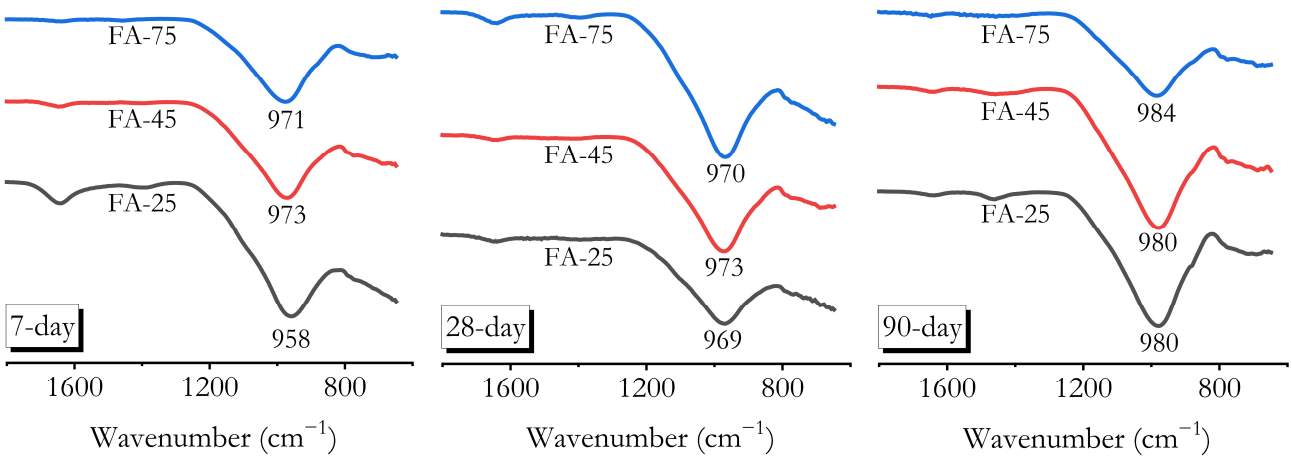

Figure 16. FTIR spectra of 7-, 28-, and 90-day FAGP samples cured under ambient, high ambient, and heat curing.

The FTIR spectra of FAGPs shown in Figure 16 display changes in the main band over time and under different curing regimes that are generally similar to those observed in PMGPs. Therefore, most of the explanations given for the PMGP spectra also apply to FAGPs. One of the key differences between the FTIR spectra of FAGP and PMGP is that, when cured at room temperature, the increase in the wavenumber at which the main band is centred over time is more pronounced in the former. This indicates that fly ash experiences significant alkali activation over time even at ambient temperature.

One of the prominent peaks apart from the main band appears around 1640 cm^{-1} in the FTIR spectra of the 7-day samples. This band corresponds to the bending vibrations of H-O-H and is typically associated with physically adsorbed water or structural water [75,76]. It is clearly visible in the samples cured at ambient temperature, moderately visible in those cured at high ambient temperature, and almost absent in heat-cured samples. This indicates that water has evaporated during heat curing. On the other hand, in all curing regimes, this band becomes less distinct at later ages beyond 7 days.

A peak around 1460 cm^{-1} is visible in the 90-day geopolymer spectra but remains indistinct in the 7- and 28-day samples. This peak is typically attributed to carbonate (CO_3^{2-}) structures formed by the reaction between free Na^+ ions in the geopolymer and atmospheric CO_2 [77]. The emergence of this band at 90 days may be due to the gradual formation and accumulation of carbonates on the surface as Na^+ ions come into contact with the environment over time. The relatively weak presence of this peak in PM-45, FA-45, and FA-75 samples may suggest that most of the Na^+ ions in these geopolymers were consumed during the geopolymerisation reactions. This is further supported by the fact that these three geopolymer mortars exhibit higher compressive strengths at 90 days compared to the others (Figure 9a,b).

3.8. Phase Identification by XRD

XRD analysis was conducted to investigate the effect of curing regimes and ageing on the mineralogical and crystalline structure development of PMGP and FAGP. Figure 17a–c presents the XRD patterns of the 7-, 28-, and 90-day samples under different curing regimes. As illustrated, the amorphous hump becomes more pronounced with time, thereby indicating enhanced geopolymerisation over time. A similar increase in the intensity of the amorphous hump due to progressive geopolymerisation was also reported by Nasaeng

et al. [78] for PMGP. Figure 18 presents the XRD patterns of the raw pumice powder and the high ambient-cured PMGP. For this comparison, a typical PMGP sample was selected, as the XRD patterns of the geopolymer specimens were generally similar to one another. As seen in Figure 18, the raw pumice powder displays a broad hump indicative of its amorphous nature, predominantly between 20° and 30° 2θ, alongside minor crystalline peaks corresponding to its inherent mineral composition. The high ambient-cured PMGP exhibits a considerably broader and more intense amorphous hump, extending approximately from 15° to 40° 2θ, suggesting an increase in amorphous phase content and the formation of a more polymerised geopolymeric network. Additionally, a distinct crystalline peak is observed in the 90-day PMGP at approximately 27° 2θ, corresponding to the formation of zeolitic phases. This zeolitic peak is evident in all 90-day PMGPs across the three curing temperatures. The formation of this phase is also clearly observable when comparing the raw pumice with 90-day PMGP at high ambient curing, as depicted in Figure 18. These findings are consistent with the observations reported by Kalatehjari et al. [28], who similarly detected zeolite crystalline phases in their XRD analyses of PMGPs. Their study argued that the use of sodium aluminate as an activator promotes zeolite formation and further explained that such formation is correlated with improvements in compressive strength development. This aligns with the compressive strength results presented in Section 3.3 of this study, thereby supporting the beneficial role of zeolite crystallisation in enhancing the mechanical performance of PMGP. Overall, the combination of the increased amorphous structure and the formation of useful crystalline phases such as zeolites highlights the effective activation process and structural improvement achieved within these PMGP.

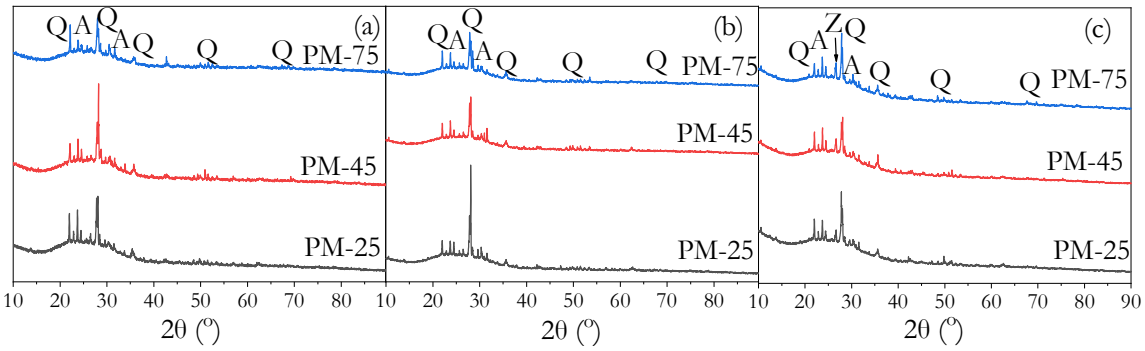

Figure 17. X-ray diffraction patterns of 7- 28- and 90-day PMGPs at ambient, high ambient, and heat curing 7-day (**a**), 28-day (**b**), 90-day (**c**). Q = quartz, A = albite, Z = zeolite.

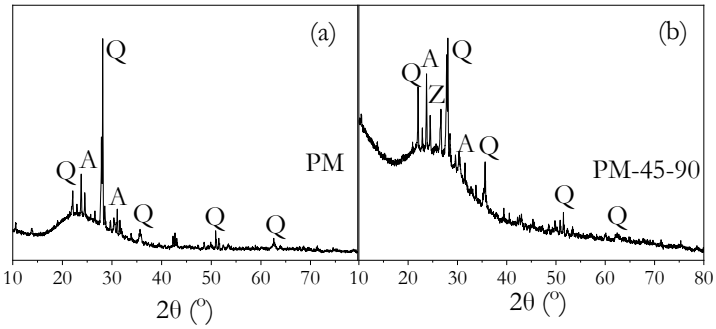

Figure 18. XRD patterns of raw pumice (**a**) and 90-day PMGP at high ambient curing (**b**). Q = quartz, A = albite, Z = zeolite.

Figure 19a–c illustrates the XRD patterns of 7-, 28-, and 90-day FAGP cured at ambient temperature, high ambient temperature (45 °C), and heat curing. The 7- and 28-day FAGP samples show a noticeable increase in the amorphous hump within the 2θ range

of 18–30°. This broadening indicates increased amorphous content, implying that more extensive geopolymerisation has occurred by 28 days. At 90 days, a further intensification of the amorphous region between 18° and 30° is evident, reflecting continued geopolymerisation. Ye and Radlinska [79] attributed the development of this amorphous hump within the 2θ range of 18–30°, which results from geopolymerisation, to the formation of an N-A-S-H gel network. This enhancement in amorphous content is more clearly illustrated in Figure 20, which compares the XRD pattern of the raw fly ash with that of a typical 90-day FAGP cured at high ambient temperature, clearly highlighting the structural transformations induced by geopolymerisation.

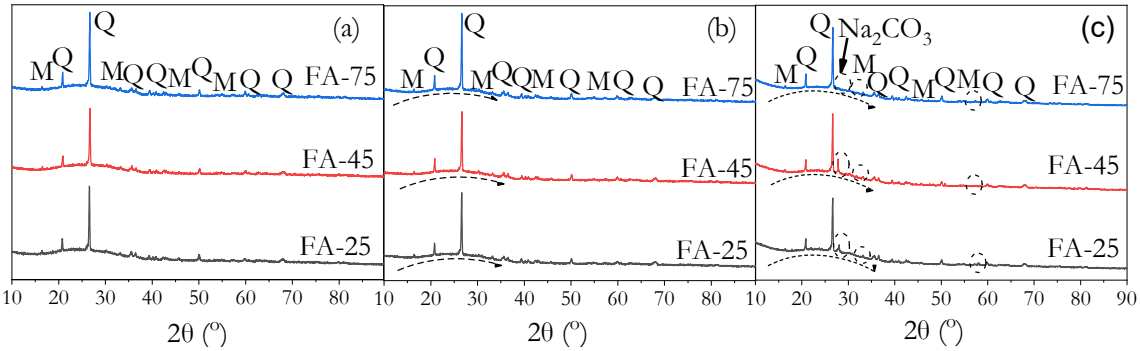

Figure 19. X-ray diffraction patterns of 7- 28- and 90-day FAGPs at ambient, high ambient, and heat curing 7-day (**a**), 28-day (**b**), 90-day (**c**). Q = quartz, M = mullite.

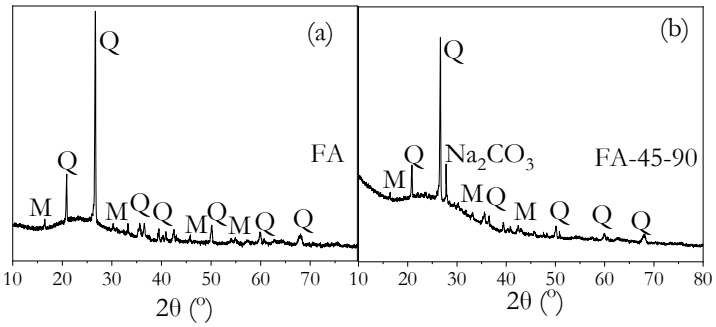

Figure 20. XRD patterns of raw fly ash (**a**) and 90-day FAGP at high ambient curing (**b**). Q = quartz, M = mullite.

Additionally, at 90 days, Na_2CO_3 peaks around 2θ = 28° were observed in samples cured at 25 °C and 45 °C. This observation may also be supported by the presence of peaks attributed to the asymmetric stretching vibration of O–C–O bonds in the FTIR spectra, as presented in Section 3.7 (Figures 15 and 16). Ge et al. [80] explained this phenomenon as likely resulting from carbonation, whereby reaction products interact with CO_2 under ambient conditions. Notably, Na_2CO_3 was not detected in samples for heat-cured FAGP. This absence of Na_2CO_3 peaks may be attributed to the accelerated reaction kinetics that densify the geopolymer matrix, thereby reducing CO_2 diffusion and subsequent carbonation. In addition, Temuujin et al. [81] reported that elevated curing temperatures can cause evaporation of moisture from the matrix, further limiting the availability of pore water necessary for carbonation reactions. For 90-day FAGP, a reduction in the intensity of mullite peaks is observed in the geopolymer matrix across all curing temperatures. In FAGP samples, mullite, identified by peaks around 2θ = 33° and 55–60°, appears to progressively dissolve with increasing curing temperature. This has been attributed to higher temperatures and sufficient curing time, which promote the breaking of Si-O and Al-O bonds and facilitate the dissolution of precursor phases. Kamwa et al. [56] reported similar

observations, noting that the dissolution of crystalline phases contributes to the development of a more cohesive geopolymer network and, consequently, improved mechanical strength. This is also confirmed in the compressive strength (Section 3.3). In contrast, the intensity of quartz peaks remains largely unchanged across curing temperatures, which is consistent with Latifi et al. [82], who emphasised that quartz, being an inert mineral, exhibits high resistance to dissolution under these conditions [83]. It should be noted that the reduction in crystallinity, particularly the dissolution of mullite, was not apparent at 7- and 28-day FAGPs. This can be attributed to the refractory nature of mullite, which requires both elevated temperatures and prolonged times to dissolve. At early curing stages, geopolymerisation is still in progress, and reaction kinetics may not be sufficient to facilitate the breakdown of stable crystalline phases. Moreover, the relatively low intensity of these phases and potential detection limits in early stages may further obscure observable changes. This prolonged reaction behaviour is also supported by Duxson et al. [84], who reported that geopolymerisation continues well beyond the initial setting time, as confirmed by calorimetric studies.

3.9. Pore Structure Evaluation via MIP

Figure 21 presents the pore size distribution and total porosity of 90-day PMGP samples cured under different regimes, as determined by mercury intrusion porosimetry (MIP). In the sample cured at ambient temperature, a significant portion of the pore structure consists of pores with diameters between 10 nm and 50 nm, while the remainder is mainly composed of pores larger than 100 nm. In the PMGP cured at high ambient temperature, pores larger than 70 nm are observed, whereas in the heat-cured sample, the vast majority of pores range between 100 nm and 400 nm (Figure 21a). The total porosity values for the PMGP samples cured at ambient temperature, high ambient temperature, and under heat curing are 8.75%, 6.02%, and 13.02%, respectively (Figure 21b).

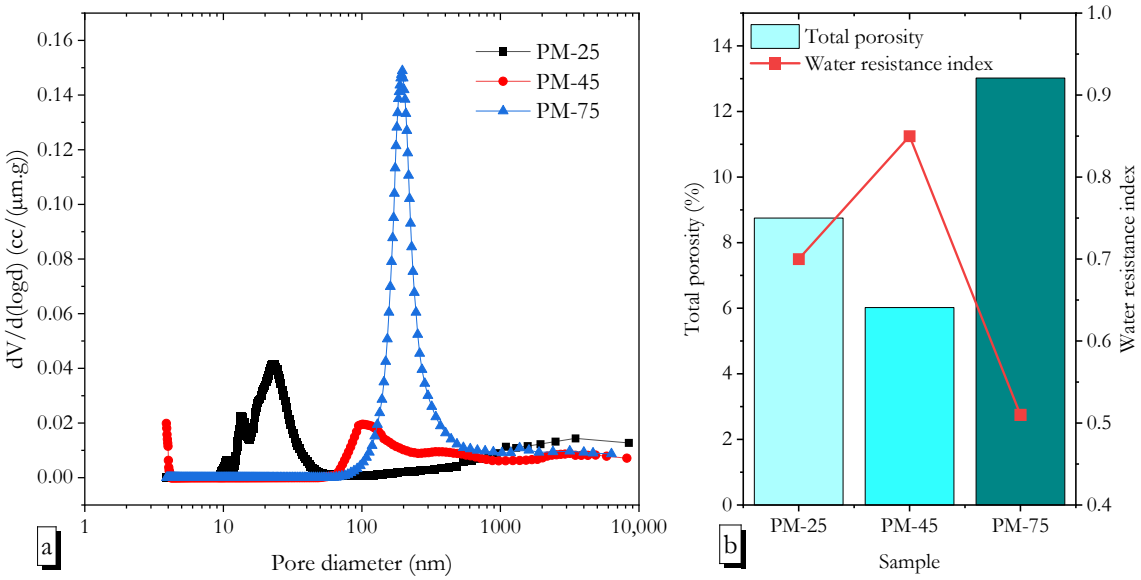

Figure 21. Pore size distribution (**a**) and total porosity values (**b**) of 90-day PMGP samples cured under ambient, high ambient, and heat curing.

The curing temperature is one of the main factors influencing the pore structure of geopolymer materials [85]. In general, heat curing at high temperatures leads to rapid water evaporation at early ages, resulting in the formation of large pores in the geopolymer matrix [46]. Moreover, due to the accelerated geopolymer reactions at high temperatures, water may be expelled from the geopolymeric network before it can be effectively bound,

further contributing to pore formation [48]. As a result, heat-cured PMGP exhibits a significantly higher proportion of large pores (greater than 100 nm) compared to the other two PMGP samples. In contrast, ambient-cured geopolymers do not experience early-stage water loss; therefore, large pores are not formed. However, the slower and more limited geopolymerisation at low temperatures means that capillary pores cannot be sufficiently filled. Consistent with this, Figure 21a shows that ambient-cured PMGP contains considerably more capillary pores (less than 100 nm) than the other two samples cured at higher temperatures. On the other hand, high ambient-cured PMGP, cured at a moderate temperature (45 °C), does not develop the large pores typical of high-temperature curing [53]. Additionally, the continued exposure to this temperature over 90 days promotes gel formation, which substantially reduces the amount of capillary porosity. Consequently, high ambient-cured PMGP has a lower total porosity than the others. Therefore, it can be concluded that applying high ambient temperatures is highly effective in reducing the porosity of geopolymers.

As explained in Section 3.4, the wet strength of both ambient-cured and heat-cured PMGP is considerably lower than their dry strength, which is largely attributed to porosity. As shown in Figure 21b, there is a strong inverse correlation between porosity and the water resistance index. This indicates that higher porosity increases the interaction of water molecules with the gel structure, reduces cohesion between solid particles, and consequently lowers strength. Accordingly, the high ambient-cured PMGP mortar, which exhibits the lowest porosity, achieved the highest resistance to water.

4. Conclusions

This study investigated the effectiveness of high-ambient-temperature curing in developing low-calcium geopolymers based on pumice (PMGP) and fly ash (FAGP), in comparison with ambient and heat curing conditions. Based on the experimental results, the following conclusions can be drawn:

1. High ambient curing allowed low-calcium geopolymers to set within 80–90 min, offering a significant advantage for in situ applications compared to ambient-cured samples, which took over 24 h.
2. Low-calcium geopolymers cured at high ambient temperatures exhibited lower water absorption than those cured under other regimes, while their sorptivity was similar to heat-cured specimens.
3. High-ambient-temperature curing was more advantageous than heat curing in terms of long-term strength for PMGP, whereas FAGP showed comparable performance even at early ages. PMGP cured at high ambient temperature achieved a 90-day strength of 57.3 MPa, which is 28.0% higher than its heat-cured counterpart. In contrast, FAGP reached 40.3 MPa at 3 days (comparable to heat-cured samples) and 57.2 MPa at 7 days, 24.2% higher than heat-cured FAGP.
4. Compressive strength measurements in the wet state after exposure to tap water, 5 wt.% sulphuric acid, and 5 wt.% hydrochloric acid showed that high ambient-cured PMGP and FAGP, as well as heat-cured FAGP, retained strengths close to their dry-state values. This indicates the formation of a robust geopolymer gel.
5. Geopolymers with high initial compressive strength generally demonstrated better freeze–thaw resistance. However, high ambient-cured PMGP, which had lower early strength (28-day), was not resistant to freeze–thaw cycles.
6. FTIR, XRD, and MIP analyses confirmed that high ambient curing sustained geopolymerisation over 90 days without forming the harmful pores often associated with heat curing. The continuous formation of geopolymer gels filled capillary pores, reducing

both their volume and connectivity, leading to a more refined pore structure compared to ambient-cured samples.

The results show that high-ambient-temperature curing is highly effective for improving long-term strength in PMGP and can eliminate the need for heat curing in FAGP by providing comparable or superior early-age performance. These materials can be used for in situ applications in hot climates, offering a cost-effective and eco-friendly alternative. Future studies should focus on the performance of such geopolymers under actual field conditions in hot regions.

Author Contributions: Conceptualization, C.K. and C.T.; methodology, C.K. and C.T.; validation, C.K. and C.T.; formal analysis, C.K. and C.T.; investigation, C.K., Ş.Ş. and C.T.; data curation, C.K., Ş.Ş. and C.T.; writing—original draft, C.K., Ş.Ş. and C.T.; writing—review and editing, C.K. and C.T.; visualisation, C.K. and C.T.; supervision, C.K. and C.T. All authors have read and agreed to the published version of the manuscript.

Funding: This research received no external funding.

Data Availability Statement: The data presented in this study are available on request from the corresponding authors.

Conflicts of Interest: The authors declare no conflict of interest.

References

1. Hwang, C.-L.; Vo, D.-H.; Tran, V.-A.; Yehualaw, M.D. Effect of high MgO content on the performance of alkali-activated fine slag under water and air curing conditions. *Constr. Build. Mater.* **2018**, *186*, 503–513. [CrossRef]
2. Balun, B.; Karataş, M. Influence of curing conditions on pumice-based alkali activated composites incorporating Portland cement. *J. Build. Eng.* **2021**, *43*, 102605. [CrossRef]
3. Ayeni, O.; Onwualu, A.P.; Boakye, E. Characterization and mechanical performance of metakaolin-based geopolymer for sustainable building applications. *Constr. Build. Mater.* **2021**, *272*, 121938. [CrossRef]
4. Albidah, A.; Alqarni, A.S.; Abbas, H.; Almusallam, T.; Al-Salloum, Y. Behavior of Metakaolin-Based geopolymer concrete at ambient and elevated temperatures. *Constr. Build. Mater.* **2022**, *317*, 125910. [CrossRef]
5. Kürklü, G. The effect of high temperature on the design of blast furnace slag and coarse fly ash-based geopolymer mortar. *Compos. Part B Eng.* **2016**, *92*, 9–18. [CrossRef]
6. Atiş, C.; Görür, E.B.; Karahan, O.; Bilim, C.; İlkentapar, S.; Luga, E. Very high strength (120 MPa) class F fly ash geopolymer mortar activated at different NaOH amount, heat curing temperature and heat curing duration. *Constr. Build. Mater.* **2015**, *96*, 673–678. [CrossRef]
7. Görhan, G.; Kürklü, G. The influence of the NaOH solution on the properties of the fly ash-based geopolymer mortar cured at different temperatures. *Compos. Part B Eng.* **2014**, *58*, 371–377. [CrossRef]
8. Zakka, W.P.; Lim, N.H.A.S.; Khun, M.C. A scientometric review of geopolymer concrete. *J. Clean. Prod.* **2021**, *280*, 124353. [CrossRef]
9. Zhuang, X.Y.; Chen, L.; Komarneni, S.; Zhou, C.H.; Tong, D.S.; Yang, H.M.; Yu, W.H.; Wang, H. Fly ash-based geopolymer: Clean production, properties and applications. *J. Clean. Prod.* **2016**, *125*, 253–267. [CrossRef]
10. Hamid, M.A.; Yaltay, N.; Türkmenoğlu, M. Properties of pumice-fly ash based geopolymer paste. *Constr. Build. Mater.* **2022**, *316*, 125665. [CrossRef]
11. Bagci, C.; Kafkas, D.; Samuel, D.M.; Kriven, W.M. Sustainable activation of pumice with partially variable substitutions of metakaolin and/or fumed silica. *Int. J. Appl. Ceram. Technol.* **2024**, *21*, 818–828. [CrossRef]
12. John, S.K.; Nadir, Y.; Girija, K. Effect of source materials, additives on the mechanical properties and durability of fly ash and fly ash-slag geopolymer mortar: A review. *Constr. Build. Mater.* **2021**, *280*, 122443. [CrossRef]
13. Pangdaeng, S.; Phoo-ngernkham, T.; Sata, V.; Chindaprasirt, P. Influence of curing conditions on properties of high calcium fly ash geopolymer containing Portland cement as additive. *Mater. Des.* **2014**, *53*, 269–274. [CrossRef]
14. Karaaslan, C. Enhancing Early Strength Development of Alkali-Activated Slag through Preheating of Materials. *Çukurova Univ. Mühendislik Fakültesi Derg.* **2023**, *38*, 1129–1138. [CrossRef]
15. Yılmaz, A.; Degirmenci, F.N.; Aygörmez, Y. Effect of initial curing conditions on the durability performance of low-calcium fly ash-based geopolymer mortars. *Bol. Soc. Esp. Ceram. Y Vidr.* **2023**, *63*, 238–254. [CrossRef]

16. Safari, Z.; Kurda, R.; Al-Hadad, B.; Mahmood, F.; Tapan, M. Mechanical characteristics of pumice-based geopolymer paste. *Resour. Conserv. Recycl.* **2020**, *162*, 105055. [CrossRef]
17. Mobasheri, F.; Shirzadi Javid, A.A.; Mirvalad, S.; Azizi, S.; Mowlaei, R. Durability and mechanical properties of pumice-based geopolymers: A sustainable material for future. *Iran. J. Sci. Technol. Trans. Civ. Eng.* **2022**, *46*, 223–235. [CrossRef]
18. Yener, E.; Karaaslan, C. Curing Time and Temperature Effect on the Resistance to Wet-Dry Cycles of Fly Ash Added Pumice Based Geopolymer. *Cem. Based Compos.* **2020**, *1*, 19–25. [CrossRef]
19. Sajan, P.; Jiang, T.; Lau, C.; Tan, G.; Ng, K. Combined effect of curing temperature, curing period and alkaline concentration on the mechanical properties of fly ash-based geopolymer. *Clean. Mater.* **2021**, *1*, 100002. [CrossRef]
20. Abdulsahib, S.M.; Zubaidi, S.L.; Almamalachy, Y.; Dulaimi, A. Temperature and precipitation change assessment in the North of Iraq using LARS-WG and CMIP6 models. *Water* **2024**, *16*, 2869. [CrossRef]
21. Rashad, A.M.; Essa, G.M. Effect of ceramic waste powder on alkali-activated slag pastes cured in hot weather after exposure to elevated temperature. *Cem. Concr. Compos.* **2020**, *111*, 103617. [CrossRef]
22. Morsy, M.; Rashad, A.M.; Shoukry, H.; Mokhtar, M.; El-Khodary, S. Development of lime-pozzolan green binder: The influence of anhydrous gypsum and high ambient temperature curing. *J. Build. Eng.* **2020**, *28*, 101026. [CrossRef]
23. Turan, C.; Javadi, A.; Consoli, N.C.C.; Turan, C.; Vinai, R.; Cuisinier, O.; Russo, G. Mechanical properties of calcareous fly ash stabilized soil. In Proceedings of the Eurocoalash 2019, Dundee, Scotland, 10–12 June 2019; pp. 184–194.
24. Rashad, A.M. An overview of pumice stone as a cementitious material–the best manual for civil engineer. *Silicon* **2021**, *13*, 551–572. [CrossRef]
25. Occhipinti, R.; Stroscio, A.; Finocchiaro, C.; Fugazzotto, M.; Leonelli, C.; Faro, M.J.L.; Megna, B.; Barone, G.; Mazzoleni, P. Alkali activated materials using pumice from the Aeolian Islands (Sicily, Italy) and their potentiality for cultural heritage applications: Preliminary study. *Constr. Build. Mater.* **2020**, *259*, 120391. [CrossRef]
26. Karaaslan, C.; Yener, E.; Bağatur, T.; Polat, R. Improving the durability of pumice-fly ash based geopolymer concrete with calcium aluminate cement. *J. Build. Eng.* **2022**, *59*, 105110. [CrossRef]
27. Karaaslan, C.; Yener, E.; Bağatur, T.; Polat, R.; Gül, R.; Alma, M.H. Synergic effect of fly ash and calcium aluminate cement on the properties of pumice-based geopolymer mortar. *Constr. Build. Mater.* **2022**, *345*, 128397. [CrossRef]
28. Kalatehjari, R.; Najafi, E.K.; Asadi, A.; Brook, M. New Zealand pumicite as a precursor in producing alkaline cement with aluminate-based activators. *Case Stud. Constr. Mater.* **2024**, *21*, e04008. [CrossRef]
29. *TS-EN-196-1*; Çimento Deney Metotları—Bölüm 1: Dayanım Tayini (Methods of Testing Cement—Part 1: Determination of Strength). TSE: Ankara, Turkey, 2016.
30. Karaaslan, C.; Yener, E. The Effect of Alkaline Activator Components on the Properties of Fly Ash Added Pumice Based Geopolymer. *J. Inst. Sci. Technol.* **2021**, *11*, 1255–1269. [CrossRef]
31. Aliabdo, A.A.; Abd Elmoaty, M.; Salem, H.A. Effect of cement addition, solution resting time and curing characteristics on fly ash based geopolymer concrete performance. *Constr. Build. Mater.* **2016**, *123*, 581–593. [CrossRef]
32. Nagalia, G.; Park, Y.; Abolmaali, A.; Aswath, P. Compressive strength and microstructural properties of fly ash–based geopolymer concrete. *J. Mater. Civ. Eng.* **2016**, *28*, 04016144. [CrossRef]
33. *TS-EN-196-3*; Çimento Deney Metotları—Bölüm 3: Priz Süreleri ve Genleşme Tayini (Methods of Testing Cement—Part 3: Determination of Setting Times and Sondness). TSE: Ankara, Turkey, 2017.
34. *TS-EN-1015-10/A1*; Kâgir Harcı-Deney Metotları—Bölüm 10: Sertleşmiş Harcın Boşluklu Kuru Birim Hacim Kütlesinin Tayini (Methods of Test for Mortar for Masonry—Part 10: Determination of Dry Bulk Density of Hardened Mortar). TSE: Ankara, Turkey, 2007.
35. *TS-EN-13057*; Beton Yapılar—Koruma ve Tamir Için Mamul ve Sistemler—Deney Metotları—Kılcal su Emmeye Direncin Tayini (Products and Systems for the Protection and Repair of Concrete Structures—Test Methods—Determination of Resistance of Capillary Absorption). TSE: Ankara, Turkey, 2002.
36. Rees, C.A.; Provis, J.L.; Lukey, G.C.; van Deventer, J.S. Attenuated total reflectance fourier transform infrared analysis of fly ash geopolymer gel aging. *Langmuir* **2007**, *23*, 8170–8179. [CrossRef]
37. Tchadjié, L.; Djobo, J.; Ranjbar, N.; Tchakouté, H.; Kenne, B.D.; Elimbi, A.; Njopwouo, D. Potential of using granite waste as raw material for geopolymer synthesis. *Ceram. Int.* **2016**, *42*, 3046–3055. [CrossRef]
38. *ASTM-666*; Standard Test Method for Resistance of Concrete to Rapid Freezing and Thawing. American Society for Testing and Materials: West Conshohocken, PA, USA, 2003.
39. Erdoğan, T.Y. *Beton (Concrete)*, 6th ed.; METU Press Publishing Company: Ankara, Turkey, 2016.
40. Mehta, P.K.; Monteiro, P.J. *Concrete: Microstructure, Properties, and Materials*; McGraw-Hill Education: New York, NY, USA, 2014.
41. Kuri, J.C.; Khan, M.N.N.; Sarker, P.K. Fresh and hardened properties of geopolymer binder using ground high magnesium ferronickel slag with fly ash. *Constr. Build. Mater.* **2021**, *272*, 121877. [CrossRef]
42. Hardjito, D.; Cheak, C.C.; Ing, C.H.L. Strength and setting times of low calcium fly ash-based geopolymer mortar. *Mod. Appl. Sci.* **2008**, *2*, 3–11. [CrossRef]

43. Tchakoute, H.; Elimbi, A.; Yanne, E.; Djangang, C. Utilization of volcanic ashes for the production of geopolymers cured at ambient temperature. *Cem. Concr. Compos.* **2013**, *38*, 75–81. [CrossRef]
44. Aldawsari, S.; Kampmann, R.; Harnisch, J.; Rohde, C. Setting time, microstructure, and durability properties of low calcium fly ash/slag geopolymer: A review. *Materials* **2022**, *15*, 876. [CrossRef]
45. Topark-Ngarm, P.; Chindaprasirt, P.; Sata, V. Setting time, strength, and bond of high-calcium fly ash geopolymer concrete. *J. Mater. Civ. Eng.* **2015**, *27*, 04014198. [CrossRef]
46. Heah, C.; Kamarudin, H.; Al Bakri, A.M.; Binhussain, M.; Luqman, M.; Nizar, I.K.; Ruzaidi, C.; Liew, Y. Effect of curing profile on kaolin-based geopolymers. *Phys. Procedia* **2011**, *22*, 305–311. [CrossRef]
47. Djobo, J.N.Y.; Elimbi, A.; Tchakouté, H.K.; Kumar, S. Mechanical properties and durability of volcanic ash based geopolymer mortars. *Constr. Build. Mater.* **2016**, *124*, 606–614. [CrossRef]
48. Zhang, M.; Zhao, M.; Zhang, G.; Sietins, J.M.; Granados-Focil, S.; Pepi, M.S.; Xu, Y.; Tao, M. Reaction kinetics of red mud-fly ash based geopolymers: Effects of curing temperature on chemical bonding, porosity, and mechanical strength. *Cem. Concr. Compos.* **2018**, *93*, 175–185. [CrossRef]
49. *TS-EN-1504-3*; Beton Yapıların Korunması ve Tamiri Için Mamuller ve Sistemler—Tarifler, Gerekler, Kalite Kontrol ve Uygunluk Değerlendirmesi—Bölüm 3: Yapisal Olan ve Yapısal Olmayan Tamir (Products and Systems for the Protection and Repair of Concrete Structures—Definitions, Requirements, Quality Control and Evaluation of Conformity—Part 3: Structural and Non-Structural Repair). TSE: Ankara, Turkey, 2006.
50. Zhao, R.; Yuan, Y.; Cheng, Z.; Wen, T.; Li, J.; Li, F.; Ma, Z.J. Freeze-thaw resistance of Class F fly ash-based geopolymer concrete. *Constr. Build. Mater.* **2019**, *222*, 474–483. [CrossRef]
51. Park, S.; Pour-Ghaz, M. What is the role of water in the geopolymerization of metakaolin? *Constr. Build. Mater.* **2018**, *182*, 360–370. [CrossRef]
52. Karaaslan, C. Unary, binary and ternary use of slag, nano-$CaCO_3$, and cement to enhance freeze-thaw durability in fly ash-based geopolymer concretes. *J. Build. Eng.* **2025**, *99*, 111631. [CrossRef]
53. Rovnaník, P. Effect of curing temperature on the development of hard structure of metakaolin-based geopolymer. *Constr. Build. Mater.* **2010**, *24*, 1176–1183. [CrossRef]
54. Kuenzel, C.; Ranjbar, N. Dissolution mechanism of fly ash to quantify the reactive aluminosilicates in geopolymerisation. *Resour. Conserv. Recycl.* **2019**, *150*, 104421. [CrossRef]
55. Rabie, M.; Irshidat, M.R.; Al-Nuaimi, N. Ambient and Heat-Cured Geopolymer Composites: Mix Design Optimization and Life Cycle Assessment. *Sustainability* **2022**, *14*, 4942. [CrossRef]
56. Kamwa, R.A.T.; Tome, S.; Nemaleu, J.G.D.; Noumbissie, L.T.; Tommes, B.; Eguekeng, I.; Spieß, A.; Woschko, D.; Chongouang, J.; Janiak, C.; et al. Effect of Curing Temperature on Properties of Compressed Lateritic Earth Bricks Stabilized with Natural Pozzolan-Based Geopolymer Binders Synthesized in Acidic and Alkaline Media. *Arab. J. Sci. Eng.* **2023**, *48*, 16151–16165. [CrossRef]
57. Mo, B.-H.; Zhu, H.; Cui, X.-M.; He, Y.; Gong, S.-Y. Effect of curing temperature on geopolymerization of metakaolin-based geopolymers. *Appl. Clay Sci.* **2014**, *99*, 144–148. [CrossRef]
58. Hou, Y.; Wang, D.; Zhou, W.; Lu, H.; Wang, L. Effect of activator and curing mode on fly ash-based geopolymers. *J. Wuhan Univ. Technol. Mater. Sci. Ed.* **2009**, *24*, 711–715. [CrossRef]
59. Hajimohammadi, A.; Provis, J.L.; Van Deventer, J.S. Effect of alumina release rate on the mechanism of geopolymer gel formation. *Chem. Mater.* **2010**, *22*, 5199–5208. [CrossRef]
60. Mindess, S.; Young, F.; Darwin, D. *Concrete*, 2nd ed.; Prentice-Hall: Upper Saddle River, NJ, USA, 2003.
61. Neville, A.M. *Properties of Concrete*; Longman: London, UK, 1995; Volume 4.
62. Redden, R.; Neithalath, N. Microstructure, strength, and moisture stability of alkali activated glass powder-based binders. *Cem. Concr. Compos.* **2014**, *45*, 46–56. [CrossRef]
63. Fu, Y.; Cai, L.; Yonggen, W. Freeze–thaw cycle test and damage mechanics models of alkali-activated slag concrete. *Constr. Build. Mater.* **2011**, *25*, 3144–3148. [CrossRef]
64. Javed, U.; Shaikh, F.U.A.; Sarker, P.K. Corrosive effect of HCl and H_2SO_4 exposure on the strength and microstructure of lithium slag geopolymer mortars. *Constr. Build. Mater.* **2024**, *411*, 134588. [CrossRef]
65. Bakharev, T. Resistance of geopolymer materials to acid attack. *Cem. Concr. Res.* **2005**, *35*, 658–670. [CrossRef]
66. Karaaslan, C.; Yener, E.; Bağatur, T.; Polat, R.; Gül, R. Uçucu kül ve kalsiyum alüminat çimentosu katkılı pomza esaslı geopolimer harçların sülfürik asit direnci. *J. Inst. Sci. Technol.* **2022**, *12*, 2302–2312. [CrossRef]
67. Vafaei, M.; Allahverdi, A.; Dong, P.; Bassim, N. Acid attack on geopolymer cement mortar based on waste-glass powder and calcium aluminate cement at mild concentration. *Constr. Build. Mater.* **2018**, *193*, 363–372. [CrossRef]
68. Mehta, A.; Siddique, R. Sulfuric acid resistance of fly ash based geopolymer concrete. *Constr. Build. Mater.* **2017**, *146*, 136–143. [CrossRef]

69. Zhang, N.; Hedayat, A.; Figueroa, L.; Steirer, K.X.; Li, H.; Sosa, H.G.B.; Bernal, R.P.H.; Tupa, N.; Morales, I.Y.; Loza, R.S.C. Experimental studies on the durability and leaching properties of alkali-activated tailings subjected to different environmental conditions. *Cem. Concr. Compos.* **2022**, *130*, 104531. [CrossRef]
70. Ribeiro, M.G.S.; Ribeiro, M.G.S.; Keane, P.F.; Sardela, M.R.; Kriven, W.M.; Ribeiro, R.A.S. Acid resistance of metakaolin-based, bamboo fiber geopolymer composites. *Constr. Build. Mater.* **2021**, *302*, 124194. [CrossRef]
71. Rees, C.A.; Provis, J.L.; Lukey, G.C.; van Deventer, J.S. In situ ATR-FTIR study of the early stages of fly ash geopolymer gel formation. *Langmuir* **2007**, *23*, 9076–9082. [CrossRef]
72. Wetzel, A.; Middendorf, B. Influence of silica fume on properties of fresh and hardened ultra-high performance concrete based on alkali-activated slag. *Cem. Concr. Compos.* **2019**, *100*, 53–59. [CrossRef]
73. Fernández-Jiménez, A.; Palomo, A. Mid-infrared spectroscopic studies of alkali-activated fly ash structure. *Microporous Mesoporous Mater.* **2005**, *86*, 207–214. [CrossRef]
74. Fernández-Jiménez, A.; Palomo, Á.; Sobrados, I.; Sanz, J. The role played by the reactive alumina content in the alkaline activation of fly ashes. *Microporous Mesoporous Mater.* **2006**, *91*, 111–119. [CrossRef]
75. Zhang, Z.; Wang, H.; Provis, J.L. Quantitative study of the reactivity of fly ash in geopolymerization by FTIR. *J. Sustain. Cem. Based Mater.* **2012**, *1*, 154–166. [CrossRef]
76. Yusuf, M.O. Bond characterization in cementitious material binders using Fourier-transform infrared spectroscopy. *Appl. Sci.* **2023**, *13*, 3353. [CrossRef]
77. Pasupathy, K.; Berndt, M.; Castel, A.; Sanjayan, J.; Pathmanathan, R. Carbonation of a blended slag-fly ash geopolymer concrete in field conditions after 8 years. *Constr. Build. Mater.* **2016**, *125*, 661–669. [CrossRef]
78. Nasaeng, P.; Wongsa, A.; Cheerarot, R.; Sata, V.; Chindaprasirt, P. Strength enhancement of pumice-based geopolymer paste by incorporating recycled concrete and calcined oyster shell powders. *Case Stud. Constr. Mater.* **2022**, *17*, e01307. [CrossRef]
79. Ye, H.; Radlińska, A. Fly ash-slag interaction during alkaline activation: Influence of activators on phase assemblage and microstructure formation. *Constr. Build. Mater.* **2016**, *122*, 594–606. [CrossRef]
80. Ge, X.; Liu, Y.; Mao, Y.; Hu, X.; Shi, C. Characteristics of fly ash-based geopolymer concrete in the field for 4 years. *Constr. Build. Mater.* **2023**, *382*, 131222. [CrossRef]
81. Temuujin, J.; van Riessen, A.; Williams, R. Influence of calcium compounds on the mechanical properties of fly ash geopolymer pastes. *J. Hazard. Mater.* **2009**, *167*, 82–88. [CrossRef]
82. Latifi, N.; Meehan, C.L.; Abd Majid, M.Z.; Horpibulsuk, S. Strengthening montmorillonitic and kaolinitic clays using a calcium-based non-traditional additive: A micro-level study. *Appl. Clay Sci.* **2016**, *132–133*, 182–193. [CrossRef]
83. Turan, C.; Javadi, A.A.; Vinai, R.; Russo, G. Effects of fly ash inclusion and alkali activation on physical, mechanical, and chemical properties of clay. *Materials* **2022**, *15*, 4628. [CrossRef]
84. Duxson, P.; Fernández-Jiménez, A.; Provis, J.L.; Lukey, G.C.; Palomo, A.; van Deventer, J.S. Geopolymer technology: The current state of the art. *J. Mater. Sci.* **2007**, *42*, 2917–2933. [CrossRef]
85. Chen, S.; Ruan, S.; Zeng, Q.; Liu, Y.; Zhang, M.; Tian, Y.; Yan, D. Pore structure of geopolymer materials and its correlations to engineering properties: A review. *Constr. Build. Mater.* **2022**, *328*, 127064. [CrossRef]